

# Optimal plant water use strategies explain soil moisture variability

Maoya Bassiouni<sup>a,b,\*</sup>, Stefano Manzoni<sup>c,d</sup>, Giulia Vico<sup>a</sup>

<sup>a</sup> Department of Crop Production Ecology, Swedish University of Agricultural Sciences, 750 07 Uppsala, Sweden

<sup>b</sup> Department of Environmental Science, Policy and Management, University of California Berkeley, Berkeley, CA 94720, USA

<sup>c</sup> Department of Physical Geography, Stockholm University, 106 91 Stockholm, Sweden

<sup>d</sup> Bolin Centre for Climate Research, Stockholm University, 106 91 Stockholm, Sweden

## ARTICLE INFO

### Keywords:

Buckingham Pi  
Eco-evolutionary optimality  
Ecohydrology  
Evapotranspiration  
Hydraulic risk  
Plant functional traits  
Plant water stress  
Soil water balance

## ABSTRACT

Plant responses to water stress influence water and carbon cycles and can lead to feedbacks on climate yet characterizing these responses at ecosystem levels remains uncertain. Quantifying ecosystem-level water use strategies is complex due to challenges of upscaling plant traits and disentangling confounding environmental factors, ultimately limiting our ability to understand and anticipate global change in ecosystem dynamics and ecohydrological fluxes. We reduce the dimensionality of this problem and quantify plant water use strategies by combining plant traits with soil and climate variables into parameter groups that synthesize key eco-physiological tradeoffs. Using a parsimonious soil water balance framework, we explore variations in plant water uptake capacity, water stress responses, and water use performance via these non-dimensional parameter groups. The group characterizing the synchronization of plant water transport and atmospheric water demand emerges as the primary axis of variation in water use strategies and interacts with the group representing plant hydraulic risk tolerance, especially in arid conditions when plant water transport is limiting. Next, we show that specific plant water use strategies maximize plant water uptake (leading to carbon gain benefits) weighted by risks of water stress (leading to higher costs of water use). A model-data comparison demonstrates that these ecohydrologically optimal parameter groups capture observed soil moisture variability in 40 ecosystems and beyond aridity, rainfall frequency is an important environmental control for plant water use strategies. The emerging parsimonious link between ecohydrological performance and non-dimensional parameters provides a tractable representation of plant water use strategies, relevant to parameterize global models while accounting for ecological and evolutionary constraints on the water cycle.

## 1. Introduction

Plant-level characteristics that regulate water transport from the soil to the atmosphere and assimilation of atmospheric carbon determine tradeoffs between plant water use for growth versus water conservation for survival (Reich, 2014; Skelton et al., 2015). They also shape species composition in competitive environments (Lu et al., 2020) and ultimately influence ecosystem carbon and water fluxes. Despite increasingly available plant trait data (Kattge et al., 2020), empirical and conceptual challenges limit our ability to exploit trait data effectively beyond the plant level to improve model process representations such as gas exchanges and drought responses at the ecosystem scale (Mencuccini et al., 2019). For example, variability in trait-based plant water use strategies between and within ecosystems (Choat et al., 2012; Skelton et al., 2015) are still poorly understood. Explaining variability in

ecological constraints on the water cycle across global biomes requires a holistic theoretical basis for plant water use strategies that accounts for dynamic interactions with environmental conditions across scales (Feng et al., 2019, 2018; Kannenberg et al., 2022).

Plant functional traits vary across species and within plant functional types (Anderegg, 2015). They exhibit global eco-evolutionary patterns (Franklin et al., 2020) and trends in response to changing water availability (Trugman et al., 2020). While these traits are often coordinated (Manzoni et al., 2013b; Mencuccini et al., 2015), untangling confounding environmental effects and understanding global patterns in trait coordination at plant to ecosystem levels remain problematic (Lavergne et al., 2019). Notably, performance of plants with similar traits varies in different climates; and, vice versa, different traits can lead to similar performance under a given climate (Feng et al., 2019). Water use strategy definitions thus need to consider traits in combination with

\* Corresponding author.

E-mail address: [maoya@berkeley.edu](mailto:maoya@berkeley.edu) (M. Bassiouni).

<https://doi.org/10.1016/j.advwatres.2023.104405>

Received 2 June 2022; Received in revised form 10 January 2023; Accepted 6 February 2023

Available online 11 February 2023

0309-1708/© 2023 The Author(s). Published by Elsevier Ltd. This is an open access article under the CC BY license (<http://creativecommons.org/licenses/by/4.0/>).

soil and climatic conditions at plant-to-ecosystem levels.

Identifying combinations of traits and soil and climatic variables that best describe key eco-physiological tradeoffs can be guided by a formal search for non-dimensional parameter groups (Buckingham, 1914). Importantly, diagnosing plant water use strategies with non-dimensional numbers (without units) provides a universal description of the system at any organizational scale and offers avenues to test hypotheses in a lower-dimensional context (Porporato, 2022). Furthermore, ecohydrological coordination embedded in the non-dimensional framework reduces equifinality and uncertainties inherent in characterizing trait-based ecological functions at plant-to-ecosystem levels in a changing climate. Non-dimensional groups have been previously used to classify plant drought responses (Feng et al., 2018), but have yet to be implemented in a modeling framework to predict drought responses in different ecosystems as well as define which specific plant water use strategies are ecohydrologically successful.

Specific strategies or plant functions emerging from trait coordination and interactions with environmental conditions can be estimated from eco-evolutionary optimality (Franklin et al., 2020; Manzoni et al., 2014). Importantly, theoretical optimality principles are applicable at both species and ecosystem levels and can improve upon empirical model formulations and reduce the number of required parameters (Harrison et al., 2021). The ability of optimality principles to explain patterns in water use strategies of whole ecosystems still needs to be further confirmed by confronting their predictions with key measured hydrologic variables.

Soil moisture integrates hydrologic fluxes, soil, plant traits, and climatic conditions that are tightly linked to ecosystem functioning (Rodríguez-Iturbe and Porporato, 2005). Soil moisture observations therefore encode plant water use patterns imposed by climatic and soil conditions, and these patterns can be interrogated via ecohydrological approaches (Bassiouni et al., 2020, 2018). Further, ecohydrological approaches accounting for the stochasticity of rainfall can characterize the mean intensity, duration, and frequency of periods of soil water deficit to identify optimal environmental conditions for vegetation (Porporato et al., 2001). Nevertheless, despite previous data-driven (Bassiouni et al., 2020) and theoretical (Manzoni et al., 2014) analyses, we lack tractable and transferable quantification of plant water use strategy patterns across biomes. To inform parametrization of plant responses to drought and anticipate ecosystem vulnerabilities to global change, we propose and test an ecohydrological optimality criterion to quantify plant water use strategies as a function of readily available environmental conditions. This theoretical approach has the advantage of being more tractable and explainable than empirical parameterizations and does not require calibration to targets such as observations of evapotranspiration and gross primary productivity.

By combining ecohydrological optimality with the Buckingham- $\Pi$  Theorem, we address the challenge of quantifying the multiple dimensions of plant water use strategies and their tradeoffs, especially at the ecosystem level. Specifically, we first reduce the complexity of eco-physiological controls on transpiration by combining plant traits with soil and climate parameters into non-dimensional  $\Pi$  groups. We then define metrics of plant water use capacity, sensitivity to water stress, and water use performance linked to daily soil moisture dynamics and long-term risks of plant water stress. Leveraging this framework and soil moisture data from 40 ecosystems, we provide data-driven and theoretical support for the hypothesis that plants adapt to long-term growing season conditions by balancing maximization of water uptake (leading to carbon gains and growth) with minimization of risks of unfavorable water-stressed conditions (leading to higher costs or penalties of water use).

Our approach extends the analytical value of non-dimensional groups beyond summarizing how traits, soil, and climate co-determine water use strategies, by implementing non-dimensional groups in an ecohydrological modeling framework to explain variability in ecological

constraints on the water cycle. Further, the framework incorporates traits into response-based metrics of plant water use strategies and link them to ecohydrological performance accounting for cumulative impacts of water stress on plant function as well as their feedbacks. This study offers a parsimonious but effective alternative to more complex models to investigate and parameterize water use strategies across wet to arid ecosystems, exploiting ecohydrological optimality as a guiding principle.

## 2. Materials and methods

Our modeling framework is centered around a conceptual representation of the soil-plant-atmosphere continuum (SPAC) (referred to as ‘eco-physiological’ model) coupled to a stochastic soil water balance (referred to as ‘ecohydrological’ model). The eco-physiological model (Section 2.1) calculates transpiration as a function of soil saturation, plant functional traits and plant hydraulic status (Fig. 1a), which we simplify to express metrics of plant water uptake capacity as a function of non-dimensional parameter groups (Fig. 1b). We then integrate the eco-physiological model into the ecohydrological model (Section 2.2) to link plant controls on transpiration to soil and climatic conditions. The coupled models quantify how biotic and abiotic components interact and ultimately determine long-term plant water use, water stress, and water use performance (Fig. 1c). We apply this SPAC-water balance framework (Section 2.3) first to explore water use strategies theoretically and then to infer plant water use strategies from data and verify an ecohydrological optimality criterion (Fig. 1d). Model parameters and metrics characterizing plant water use strategies are summarized in Tables 1 and 2, respectively.

### 2.1. Eco-physiological model and reducing the dimensionality of plant water use strategies

The daily rate of transpiration ( $T$ ,  $\text{m day}^{-1}$ ) is bound by potential atmospheric water demand, characterized here by potential evaporation ( $E_0$ ,  $\text{m day}^{-1}$ , Priestley and Taylor, 1972) and constrained by soil water supply within a depth  $Z$  (m), characterized here by soil water saturation ( $s$ , unitless,  $0 \leq s \leq 1$ ). We aim to simplify the description and exploration of plant water use strategies by expressing the ratio  $\beta = T/E_0$  as a function of  $s$  and non-dimensional parameters that define eco-physiological tradeoffs (Fig. 1a – b). Further, we derive four metrics of plant water uptake capacity and the sensitivity of plant uptake to hydraulic status (resulting from  $E_0$  and  $s$  together) to summarize different plant water use strategies.

#### 2.1.1. Water flux through the soil-plant-atmosphere continuum (SPAC)

Following conceptual plant hydraulics models (Feng et al., 2017; Manzoni et al., 2013b), we assume plant water storage is much smaller than transpiration at the daily time scale and equate water fluxes along different components of the SPAC (Fig. 1a). Therefore,  $T$  is equal to the rate of water supply from soil to roots; water transport from roots to canopy; and water flux from canopy to the atmosphere. The rate of water supply from soil to canopy is driven by the difference between soil ( $\psi_s$ , MPa) and canopy ( $\psi_c$ , MPa) water potentials (we neglected gravimetric potential) and is controlled by the series of soil-to-root ( $K_{SR}$ ,  $\text{m day}^{-1} \text{MPa}^{-1}$ ) and plant xylem ( $K_P$ ,  $\text{m day}^{-1} \text{MPa}^{-1}$ ) conductances. The water flux from canopy to atmosphere is equal to water vapor that diffuses through stomata, driven by the difference in water vapor in the atmosphere and in the leaf ( $D$ ,  $\text{mol}^{-1}$ ), and is regulated by canopy conductance ( $G_C$ ,  $\text{m day}^{-1}$ ):

$$T = \beta(s)E_0 = \frac{K_{SR}K_P}{K_{SR} + K_P}(\psi_s - \psi_c) = G_C D. \quad (1)$$

We assume that  $K_{SR}$  decreases non-linearly with decreasing  $\psi_s$  from its maximum value  $K_{SR,max}$  at soil saturation ( $\psi_{s,sat}$ ); and that  $K_P$  and  $G_C$

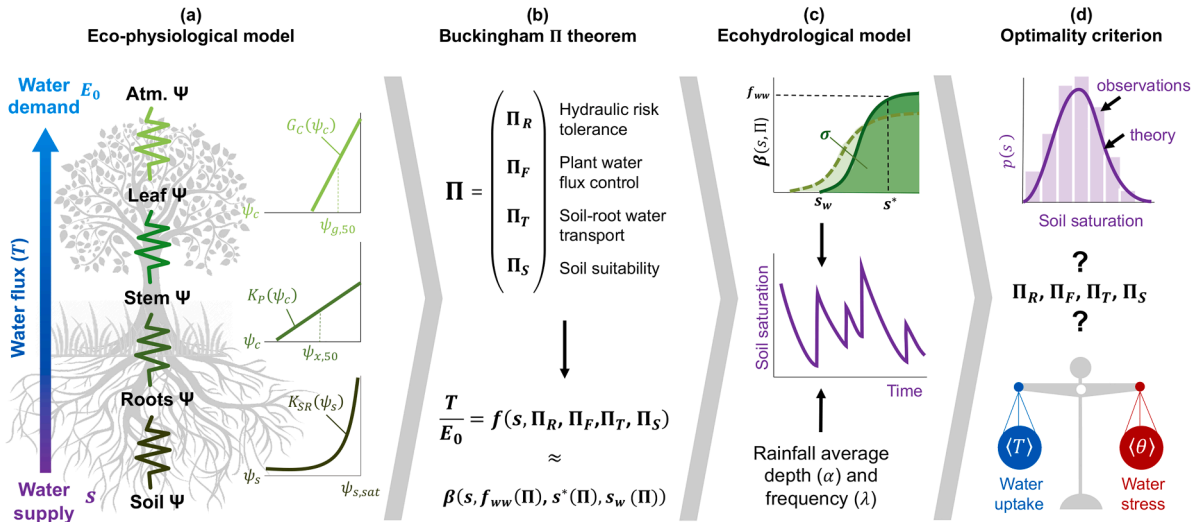


**Fig. 1.** Visual summary. (a) A series of flux-gradient relations describes the soil-plant-atmosphere continuum (SPAC). Water flux along the SPAC depends on local water potential status from the soil ( $\psi_s$ ) to the canopy ( $\psi_c$ ) and conductances of the soil and root ( $K_{SR}$ ), plant stem ( $K_P$ ), and canopy ( $G_C$ ). (b) We reduce the complexity of the SPAC by combining variables into four non-dimensional  $\Pi$  groups and express the ratio ( $\beta$ , Eq. (2)) between transpiration ( $T$ ) and atmospheric evaporative demand ( $E_0$ ) as a function of soil saturation ( $s$ ) and  $\Pi$  groups. (c) The shape of this function varies with plant water uptake capacity and can be approximated by three shape parameters ( $f_{ww}$ ,  $s^*$ ,  $s_w$  Eqs. (4) and (5)) and an overall index reflecting water use strategies from stress averse to stress tolerant ( $\sigma$ , Eq. (6)). We implement  $\beta(s, \Pi)$  in a water balance forced with stochastic rainfall (with average depth  $\alpha$  and frequency  $\lambda$ ) and obtain soil saturation probability distributions ( $p(s)$ , Eq. (8)), as well as long-term mean transpiration ( $T$ , Eq. (10)) and risk of water stress ( $\theta$ , Eq. (12)) as a function of  $\alpha$ ,  $\lambda$ ,  $\Pi$  groups, soil texture, and rooting depth. (d) We test if parameters that best-fit empirical  $p(s)$  derived from soil saturation observations also optimize plant water use performance in terms of maximizing plant water uptake weighted by risks of water stress ( $\epsilon$ , Eq. (13)).

decrease linearly with decreasing  $\psi_c$  from their maximum values  $K_{P,max}$  and  $G_{C,max}$ , respectively and with slopes determined by canopy water potentials at 50% xylem ( $\psi_{x,50}$ , MPa) and stomatal ( $\psi_{g,50}$ , MPa) conductance loss (Fig. 1a). We focus on the ecosystem as a whole and express all conductances per unit ground area. They are functions of plant root-, stem-, and leaf-level traits and soil water retention parameters (Table 1), such as root area index (RAI,  $m^2 m^{-2}$ ); leaf-specific maximum xylem conductivity ( $k_{x,max}$ ,  $kg m^{-1} MPa^{-1} s^{-1}$ ); canopy height ( $h_c$ , m); leaf area index (LAI,  $m^2 m^{-2}$ ); and saturated soil conductivity ( $k_{s,sat}$ ,  $m day^{-1}$ ) – see Manzoni et al. (2014) for details on this linearized SPAC parameterization and justifications for simplifications.

### 2.1.2. Non-dimensional groups emerging from the SPAC

Eight parameters and state variables suffice to describe key aspects of water flux through the SPAC and its sensitivity to environmental conditions defined in the eco-physiological model:  $T$ , varying with plant traits, soil texture, climate, and water status;  $E_0$ , varying here only with temperature and radiation (Priestley and Taylor, 1972);  $s$ , the only state variable in our framework, varying due to stochastic rainfall events affecting the soil water balance within a depth  $Z$  and controlled by SPAC characteristics;  $K_{SR,max}$ , varying with soil texture and root structure and depth;  $K_{P,max}$ , varying with xylem conductivity and plant size;  $\psi_{g,50}$ , varying with stomatal sensitivity;  $\psi_{x,50}$ , varying with xylem vulnerability;  $\psi_{s,sat}$ , varying with soil texture.

The dimensionality of the system can be reduced by combining these eight variables based on three primary dimensions (length, time, and mass), but only two primary units ( $m day^{-1}$  and MPa), into  $8 - 2 = 6$  non-dimensional quantities (Buckingham, 1914) that summarize key climate, soil, and eco-physiological tradeoffs emerging from the SPAC:

$\beta = T/E_0$  reflects the degree of *transpiration downregulation* and varies temporally in response to plant water stress. A value of 1 indicates transpiration is equal to potential atmospheric water demand and a value of 0 indicates transpiration has ceased.

$s$  reflects *soil water supply* relative to soil saturation within a depth  $Z$  and varies with the soil water balance driven by stochastic rainfall inputs and controlled by SPAC characteristics. A value of 1 indicates all

soil pores are filled with water and the minimum value is the hygroscopic point when water is bound to the soil.

$\Pi_R = \frac{\psi_{g,50}}{\psi_{x,50}}$  reflects the degree of plant *hydraulic risk tolerance*. A value close to 0 represents the most risk-averse strategy, with strict stomatal control to limit xylem damage; and a value close to 1 represents the most risk-tolerant strategy, with more passive stomatal control to favor carbon assimilation (Feng et al., 2018; Skelton et al., 2015).

$\Pi_F = \frac{E_0}{K_{P,max} |\psi_{g,50}|}$  reflects the degree of *plant water flux control*. A value close to 0 indicates that plant water supply is nearly unlimited compared to atmospheric demand; a value close to 1 indicates synchronization of supply and demand; and larger values point to a bottleneck in plant water transport relative to demand due to stomatal and/or xylem limitations.

$\Pi_T = \frac{K_{SR,max} |\psi_{g,50}|}{E_0}$  reflects *soil-root water transport capacity*. Values are generally high, but lower values occur when water supply is limited by the soil-root system for slow draining soils (clay).

$\Pi_S = \frac{\psi_{g,50}}{\psi_{s,sat}}$  reflects *soil suitability* for plant water extraction. Values are generally high ( $|\psi_{s,sat}|$  tends to be small) and highest values occur for high porosity soils (sand).

Applying the Buckingham-II Theorem (Buckingham, 1914; Porporato, 2022) by relating  $\beta$  to  $s$  and the four  $\Pi$  groups (Fig. 1b), we can express plant water uptake at a given soil saturation without dimensions but accounting for SPAC environmental and plant characteristic that vary across ecosystems

$$\beta = f(s, \Pi_R, \Pi_F, \Pi_T, \Pi_S). \quad (2)$$

We note that the application of Buckingham-II Theorem does not lead to a unique choice of non-dimensional groups and results are specific to the system under consideration and the line of inquiry. We obtain six groups for our simplified representation of the water flux through the SPAC and these groups have similarities to nine groups previously identified for describing plant hydraulic failure and carbon limitations due to drought stress (Feng et al., 2018). We choose  $E_0$  and  $\psi_{g,50}$  as key representative variables (to non-dimensionalize units of  $m s^{-1}$  and MPa,

**Table 1**

List of ecohydrological model state variables, parameters, symbols, and explanations. Values listed are for a baseline temperate broadleaf forest with loam soil texture used in Figs. 2–5. Subscripts denote sources of parameter values for implementing the model at study sites.

Symbol	Definition	Unit	Value
<i>State variables</i>			
$T$	Plant soil water uptake or transpiration	$\text{m s}^{-1}$	
$s$	Soil saturation or relative soil moisture	unitless	
$\theta$	Dynamic plant water stress	unitless	
$\beta$	Degree of transpiration downregulation	unitless	
<i>Physical constants</i>			
$g$	Gravitational acceleration	$\text{m s}^{-2}$	9.81
$\rho_w$	Water density	$\text{kg m}^{-3}$	1000
<i>Climate characteristics</i>			
$T_d$	Day length	$\text{s day}^{-1}$	43,200 <sup>a</sup>
$E_0$	Potential evaporation	$\text{m day}^{-1}$	0.0035 <sup>a</sup>
$\alpha$	Rainfall intensity	$\text{m day}^{-1}$	0.007 <sup>a</sup>
$\lambda$	Rainfall frequency	$\text{day}^{-1}$	0.35 <sup>a</sup>
<i>Soil texture characteristics</i>			
$k_{s,sat}$	Saturated soil hydraulic conductivity	$\text{m day}^{-1}$	0.3 <sup>a</sup>
$\psi_{s,sat}$	Soil water potential near saturation	MPa	-0.0047 <sup>a</sup>
$b$	Exponent of the soil-water retention curve	unitless	5.39 <sup>a</sup>
$s_{fc}$	Soil saturation at field capacity (-0.03 MPa)	unitless	0.71 <sup>a</sup>
$s_h$	Soil saturation at the hygroscopic point (-10 MPa)	unitless	0.24 <sup>a</sup>
$n$	Soil porosity	$\text{m}^2 \text{m}^{-2}$	0.45 <sup>a</sup>
<i>Root matrix characteristics</i>			
$Z_r$	Rooting depth	m	0.5 <sup>a</sup>
RAI	Root area index per unit ground area	$\text{m}^2 \text{m}^{-2}$	10 <sup>b</sup>
$d_r$	Fine root diameter	m	0.0005 <sup>c</sup>
<i>Canopy characteristics</i>			
LAI	Ecosystem leaf area index per unit ground area	$\text{m}^2 \text{m}^{-2}$	2 <sup>a</sup>
$\psi_{g,50}$	Canopy water potentials at 50% stomatal conductance loss	MPa	-1.5 <sup>b</sup>
$h_i$	Characteristic amount of interception per unit leaf area	$\text{m day}^{-1}$	0.0002 <sup>c</sup>
$k$	Canopy radiation extinction coefficient	unitless	1.2 <sup>c</sup>
<i>Plant stem characteristics</i>			
$h_c$	Canopy height	m	20 <sup>a</sup>
$k_{x,max}$	Leaf-specific maximum xylem hydraulic conductivity	$\text{kg m}^{-1} \text{MPa}^{-1} \text{s}^{-1}$	0.0008 <sup>b</sup>
$\psi_{x,50}$	Canopy water potentials at 50% xylem conductance loss	MPa	-2.5 <sup>b</sup>
<i>Upscaled maximum conductance per unit ground area</i>			
$K_{P,max}$	$= k_{x,max} \frac{LAI}{h_c} \frac{T_d}{\rho_w}$	$\text{m day}^{-1} \text{MPa}^{-1}$	
$K_{SR,max}$	$= k_{s,sat} \sqrt{\frac{RAI}{d_r Z_r}} \frac{10^6}{\rho_w g}$	$\text{m day}^{-1} \text{MPa}^{-1}$	

<sup>a</sup> extracted from FLUXNET2015 data and metadata (Table S1).  
<sup>b</sup> inferred from the ecohydrological model.  
<sup>c</sup> assumed constant for all ecosystems and based on literature values.

**Table 2**

Summary of non-dimensional parameters and metrics characterizing plant water use strategies and plant water use performance.

Symbol	Definition
$\Pi_R$	Plant hydraulic risk tolerance
$\Pi_F$	Plant water flux control
$\Pi_T$	Soil-root water transport capacity
$\Pi_S$	Soil suitability
$f_{ww}$	Fractional loss of conductivity in well-watered conditions (Eq. (4))
$s^*$	Soil saturation at incipient stomatal closure (Eq. (5))
$s_w$	Soil saturation when plant water uptake ceases (Eq. (5))
$\sigma$	Overall index of plant water uptake capacity (Eq. (6))
$\epsilon$	Plant water use performance (Eq. (13))

respectively) because we aim to interpret coordination of climate and stomatal sensitivity versus other SPAC characteristics. A different selection of variables and their combinations would result in less compact approximations of  $\beta$  as a function of  $s$  and  $\Pi$  groups (Eqs. (3)–(5) below). We also note that as a result of the assumption that the daily water flux through the xylem must be transpired through stomata, canopy conductance is a redundant variable and hence does not appear in  $\Pi$  groups. This does not imply that a  $\Pi$  group describing canopy conductance would be unimportant. Rather, this implies that the SPAC depends on coordination between stomatal and xylem traits and therefore we can adopt a more parsimonious description of the system without canopy

conductance and representing atmospheric water demand via only  $E_0$ . Further,  $\psi_{g,50}$  is regarded as an outcome of a specific response to plant stress rather than a prescribed trait because, as we will show, we infer  $\psi_{g,50}$  values from data-driven and optimality criteria.

### 2.1.3. Metrics of plant water uptake capacity

We approximate Eq. (2) mathematically to express key characteristics of plant water uptake capacity analytically as a function of  $\Pi$  groups. To do so, similarly to previous work (Manzoni et al., 2014), we solve the SPAC eco-physiological model (Eq. (1)) for three shape parameters of a piece-wise linear function that downregulates transpiration due to soil water stress (Feddes et al., 1978; Laio et al., 2001)

$$\beta(s, \Pi) \approx \begin{cases} 0, & s \leq s_w, \\ \frac{s - s_w}{s^* - s_w} f_{ww}, & s_w < s \leq s^*, \\ f_{ww}, & s^* < s, \end{cases} \quad (3)$$

where  $f_{ww}$  is the ratio of the well-watered rate of transpiration to  $E_0$ ;  $s^*$  and  $s_w$  are soil saturation thresholds below which transpiration is downregulated from its well-watered rate and when transpiration ceases, respectively.

By solving Eq. (1) under well-watered conditions ( $\psi_s = 0$ ) and assuming soil-to-root conductance ( $K_{SR}$ ) is not limiting, we obtain an expression for  $f_{ww}$  as a function of climate and eco-physiological

variables embedded in the  $\Pi$  groups:

$$f_{ww} = 1 - \frac{1}{2\Pi_R} \left[ 1 + \frac{\Pi_F}{2} - \sqrt{\left(\frac{\Pi_F}{2} + 1\right)^2 - 2\Pi_F\Pi_R} \right]. \quad (4)$$

By solving Eq. (1) for  $\psi_s$  at which any arbitrary transpiration rate  $T = \beta E_0$  is achieved, we can express  $s$  as a function of  $\beta$  and  $\Pi$  groups.

$$s(\beta) = \left( \frac{\psi_s(\beta)}{\psi_{s,sat}} \right)^{-\frac{1}{b}} = \left[ \frac{\Pi_F}{2\beta\Pi_S} \left( \sqrt{1 + \frac{4\beta\Pi_S^2}{\Pi_F} \left( 2(1-\beta) - \frac{\beta\Pi_F}{1-(1-\beta)\Pi_R} \right)} - 1 \right) \right]^{\frac{1}{b}}, \quad (5)$$

where  $b$  (unitless) is a soil pore size parameter for converting  $\psi_s$  to  $s$  (Brooks and Corey, 1964). The soil saturation thresholds for the piece-wise linear function (Eq. (3)) are then defined by setting  $\beta = 0.95f_{ww}$  for  $s^*$  and  $\beta = 0.05f_{ww}$  for  $s_w$  in Eq. (5), while evaluating Eq. (5) with  $\beta$  in the interval (0, 1) reproduces a sigmoidal response (Fig. 1c).

Through their dependence on  $\Pi$  groups Eq. (4) and (5),  $f_{ww}$ ,  $s^*$ , and  $s_w$  account for stomatal and hydraulic traits, plant size and density, as well as soil and climate characteristics. As such, these combined parameters lead to a certain realized water uptake capacity that reflects limitations to plant water transport along the SPAC beyond soil water availability in the rooting zone (i.e.,  $s$  or  $\psi_s$ ). We define the index  $\sigma$  (unitless) as the overall plant water uptake capacity relative to a hypothetical maximum corresponding to no hydraulic or stomatal limitation. We calculate  $\sigma$  by integrating  $\beta$  (Eq. (3)) over soil saturation states between the hygroscopic point ( $s_h$ ) and field capacity ( $s_{fc}$ ), and normalizing by the same integral when transpiration is equal to  $E_0$  for all soil saturation states

$$\sigma = f_{ww} \frac{s_{fc} - \frac{s^* + s_w}{2}}{s_{fc} - s_h}. \quad (6)$$

The shape of  $\beta(s, \Pi)$  therefore summarizes complex SPAC eco-physiological mechanisms including interactions with environmental conditions and represents water use strategies ranging from stress averse ( $\sigma$  close to 0) to stress tolerant ( $\sigma$  close to 1). This spectrum includes, for example, intensive water use when soil saturation is high ( $f_{ww}$  close to 1 and  $s^*$  much lower than  $s_{fc}$ , leading to high  $\sigma$ ); conservative water use when soil saturation is high ( $f_{ww}$  much lower than 1,  $s^*$  close to  $s_{fc}$ , leading to low  $\sigma$ ); sensitive water use when stomata rapidly close at high saturation states ( $s_w$  close to  $s^*$ , leading to low  $\sigma$ ); or extensive water use with the ability to partially open stomata at low saturation states ( $s_w$  much lower than  $s^*$ , leading to high  $\sigma$ ).

These four plant water use strategy characteristics ( $f_{ww}$ ,  $s^*$ ,  $s_w$ ,  $\sigma$ ), describing the shape of  $\beta(s, \Pi)$ , span multiple levels of abstraction that can be useful for varying levels of inquiry about plant water uptake capacity. Due to its definition as an integral,  $\sigma$  summarizes plant water use strategies from stress-averse to stress-tolerant with some equifinality. Therefore, nuanced strategies still need to be interpreted from the ecohydrological parameters ( $f_{ww}$ ,  $s^*$ ,  $s_w$ ) defining water uptake capacity along the full range of soil saturation states. At an even finer level of detail, the role of plant traits ( $\psi_{g,50}$ ,  $\psi_{x,50}$ ,  $k_{x,max}$ ,  $RAI$ ) on these strategies needs to be assessed via eco-physiological tradeoffs reflected in the  $\Pi$  groups.

Our plant water use strategy metrics, can also be interpreted along the iso to anisohydric continuum or ‘hydroscape’ (Fu and Meinzer, 2019; Meinzer et al., 2016). For example, for the same value of plant water uptake capacity ( $\sigma$ ), isohydric behavior can be associated with relatively higher  $f_{ww}$ ,  $s^*$ , and  $s_w$  (higher plant conductance but more stringent stomatal regulation), while anisohydric behavior can be associated with relatively lower  $f_{ww}$ ,  $s^*$ , and  $s_w$  (lower plant conductance and higher stomatal resistance to drying soil). We also note that definitions of  $f_{ww}$ ,  $s^*$ , and  $s_w$  parameters, which are a function of traits, soil and climate variables underline the need for cautious interpretation of isohydricity indexes with a plant’s environmental conditions (Feng

et al., 2019; Kannenberg et al., 2022).

## 2.2. Ecohydrological model and parsimonious quantification of plant water use performance

The capacity of plants to take up water, determined by  $\Pi$  groups and based on the eco-physiological model (Section 2.1), influences the soil water balance and occurrence of water stress, resulting in varying performances depending on local soil and hydro-climatic conditions. To quantify links between plant water use strategies and water use performance, we integrate our novel formulation of  $\beta(s, \Pi)$  (Eqs. (3)–(5)) in a soil water balance (Fig. 1c–d), thus constructing our ecohydrological model. The soil water balance accounts for stochastic rainfall characteristics as well as water balance components interacting with transpiration (soil water evaporation, canopy interception, runoff, and infiltration). We then obtain growing season soil saturation probability distributions ( $p(s)$ , Eq. (8), from which we can directly assess long-term average plant water uptake ( $T$ , Eq. (9)), risks of water stress ( $\theta$ , Eq. (11)), and water use performance ( $\varepsilon$ , Eq. (12)). While performance in this study is focused on water as a limiting factor, there are further avenues to additionally account for light and nutrient limitations or atmospheric CO<sub>2</sub> effects in  $\Pi$  groups through for example more complex definitions of potential atmospheric demand instead of  $E_0$  used here (Priestley and Taylor, 1972).

### 2.2.1. Stochastic soil water balance

We consider a bucket model for a homogenous soil column with a depth  $Z$  (m) and porosity  $n$  (unitless), in which water fluxes are interpreted at the daily time scale. This lumped approach employs scale-effective parameters (Bassiouni et al., 2020, 2018; Manzoni et al., 2014) and resulting fluxes represent the individual or whole ecosystem water balance, depending on the organizational scale at which the model and its parameters are interpreted. We assume that the dynamics of  $Z$  and rooting zone evapotranspiration dynamics are synchronized (Dong et al., 2022). Therefore, modeled soil water dynamics are representative of the ecosystem, even if the soil column depth, prescribed by observation depths (Table S1), may not exactly comprise the whole rooting zone. This assumption is justified by our focus on the temporal dynamics of evapotranspiration and their relation to soil saturation instead of total ecosystem evapotranspiration volume.

The daily soil water change is the difference between the rate of rainfall and the rate of soil water losses, including surface runoff, infiltration below depth  $Z$ , and evapotranspiration. We treat rainfall as a censored Poisson distribution characterized by a mean event depth ( $\alpha$ , m day<sup>-1</sup>), frequency ( $\lambda$ , day<sup>-1</sup>), and canopy interception threshold ( $\Delta$ , m day<sup>-1</sup>). Excess rainfall relative to available soil storage is converted to surface runoff according to a saturation excess mechanism; the rate of infiltration is both a stochastic process controlled by rainfall and a state-dependent process; and the rate of evapotranspiration is a state-dependent process, dependent on saturation and vegetation (Caylor et al., 2006; Laio et al., 2001).

We approximate  $\Delta$  empirically multiplying  $LAI$  by a characteristic amount of interception per unit leaf area ( $h_i = 2 \times 10^{-4}$  m day<sup>-1</sup>) (Bastiaanssen et al., 2012). The mean frequency of rainfall reaching the soil under the canopy is thus reduced to  $\lambda' = \lambda e^{-h_i LAI/\alpha}$ . We assume that vegetation canopies exponentially reduce potential energy available for soil water evaporation due to shading according to Beer’s law ( $\Phi = e^{-kLAI}$ ), where  $k = 1.2$  is an extinction coefficient ensuring that potential soil water evaporation becomes  $< 0.05E_0$  for closed canopies and relations between  $LAI$  and our modeled long-term fraction of transpiration to total evaporation (Fig. S1) reflects observed patterns (Wang et al., 2014; Wei et al., 2017). Following Caylor et al. (2006), we partition total potential soil water losses from evapotranspiration per unit ground area (bound by  $E_0$ ) into maximum soil water evaporation ( $\Phi E_0$ ) plus maximum plant water uptake ( $(1 - \Phi)E_0$ ).

As such, the total rate of soil water losses is a continuous piece-wise

function of soil saturation, including vertical drainage for states above  $s_{fc}$ ; plant water uptake, which decreases linearly from  $f_{ww}(1 - \Phi)E_0$  for states above  $s^*$  to 0 at  $s_w$  (Eq. (3)); and soil water evaporation, which decreases linearly from  $\Phi E_0$  for states above  $s_{fc}$  to 0 at  $s_h$ . The complete deterministic soil water loss function standardized by  $nZ$  (denoted by  $\rho(s)$ ) is

$$\rho(s) = \begin{cases} \eta_E + \eta_T + m \left[ e^{a(s-s_{fc})} - 1 \right], & s_{fc} < s \leq 1 \\ \eta_E \frac{s-s_h}{s_w-s_h} + \eta_T, & s^* < s \leq s_{fc}, \\ \eta_E \frac{s-s_h}{s_{fc}-s_h} + \eta_T \frac{s-s_w}{s^*-s_w}, & s_w < s \leq s^*, \\ \eta_E \frac{s-s_h}{s_{fc}-s_h}, & s_h < s \leq s_w, \\ 0, & 0 < s \leq s_h, \end{cases} \quad (7)$$

where  $\eta_E = \frac{\Phi E_0}{nZ}$ ,  $\eta_T = f_{ww} \frac{(1-\Phi)E_0}{nZ}$ ;  $a = 2b - 4$ ;  $m = \frac{k_{s,sat}}{nZ[e^{a(1-s_{fc})} - 1]}$ .

The soil saturation probability density function ( $p(s)$ ) for the homogenous soil column with maximum water storage  $nZ$  can be derived analytically given this stochastic soil water balance under the assumption of statistical steady-state during the growing season. We can thus calculate  $p(s)$  directly for given soil properties ( $n$ ,  $k_s$ ,  $s_{sat}$ ,  $b$ ,  $s_{fc}$ ,  $s_h$ ), average growing season climate ( $E_0$ ,  $\alpha$ , and  $\lambda$ ), vegetation cover ( $LAI$ ), as well as plant water use strategies (II groups). The solution for  $p(s)$  given by Caylor et al. (2006) and recast for our model variant is:

$$p(s) = C e^{-\gamma s} \rho(s) \begin{cases} (s_w - s_h)^{\kappa} \left[ \frac{s^* - s_h}{s_w - s_h} + \frac{\eta_T (s_{fc} - s_h)}{\eta_E (s_w - s_h)} \right]^{\omega} \left[ \frac{(\eta_E + \eta_T)(s_{fc} - s_h)}{\eta_E (s^* - s_h) + \eta_T (s_{fc} - s_h)} \right]^{\kappa} e^{\delta}, & s_{fc} < s \leq 1, \\ (s_w - s_h)^{\kappa} \left[ \frac{s^* - s_h}{s_w - s_h} + \frac{\eta_T (s_{fc} - s_h)}{\eta_E (s_w - s_h)} \right]^{\omega} \left[ \frac{\eta_E (s - s_h) + \eta_T (s_{fc} - s_h)}{\eta_E (s^* - s_h) + \eta_T (s_{fc} - s_h)} \right]^{\kappa}, & s^* < s \leq s_{fc}, \\ (s_w - s_h)^{\kappa} \left[ \frac{s - s_h}{s_w - s_h} + \frac{\eta_T (s - s_w)(s_{fc} - s_h)}{\eta_E (s^* - s_w)(s_w - s_h)} \right]^{\omega}, & s_w < s \leq s^*, \\ (s - s_h)^{\kappa}, & s_h < s \leq s_w, \\ 0, & 0 < s \leq s_h, \end{cases} \quad (8)$$

where  $\frac{1}{\gamma} = \frac{\alpha}{nZ}$ ;  $\kappa = \lambda' \frac{s_{fc} - s_h}{\eta_E}$ ;  $\omega = \lambda' \frac{(s_{fc} - s_h)(s^* - s_w)}{\eta_E (s^* - s_w) + \eta_T (s_{fc} - s_h)}$ ;  $\delta = \lambda' \frac{\ln \left( \frac{\rho(s)}{\eta_E + \eta_T} \right) - a(s - s_{fc})}{a(m - \eta_E - \eta_T)}$ ;  $C$  is a constant to ensure that the integral of  $p(s)$  over  $0 < s < 1$  is equal to 1.

Finally, we calculate the long-term mean growing season water balance components including precipitation ( $\langle P \rangle = \alpha \lambda$ ), soil water evaporation ( $E$ ), plant transpiration ( $T$ ), and canopy interception ( $I$ ) as

$$\langle E \rangle = \Phi E_0 \int_{s_h}^{s_{fc}} \frac{s - s_h}{s_{fc} - s_h} p(s) ds + \Phi E_0 \int_{s_{fc}}^1 p(s) ds \quad (9)$$

$$\langle T \rangle = (1 - \Phi) f_{ww} E_0 \int_{s_w}^{s^*} \frac{s - s_w}{s^* - s_w} p(s) ds + (1 - \Phi) f_{ww} E_0 \int_{s^*}^1 p(s) ds, \quad (10)$$

$$\langle I \rangle = \alpha \lambda (1 - e^{-h_i LAI / \alpha}) \quad (11)$$

where integrals on the right-hand side of Eqs. (9) and (10) represent mean  $E$  and  $T$  under water-limited and well-watered conditions, respectively. Differently from previous contributions, this water balance accounts for plant behavior ranging from stress-averse to stress-tolerant via water use strategies as a function of II groups (Eq. (4) for  $f_{ww}$  and Eq. (5) for  $s^*$  and  $s_w$ ).

### 2.2.2. Risk of plant water stress

We use dynamic plant water stress ( $\theta$ ), proposed in Porporato et al. (2001), to quantify long-term risk of water stress using the stochastic soil water balance. This metric accounts for the impact of stress (stomatal closure) and its likelihood (occurrence of soil saturation states below  $s^*$ ), which are quantified via long-term mean static plant stress ( $\zeta$ , unitless), as well as the number ( $n_*$ , unitless) and duration ( $T_*$ , days) of soil saturation crossings of the  $s^*$  threshold during the growing season

$$\langle \theta \rangle = \min \left[ \left( \frac{\langle \zeta \rangle \langle T_* \rangle}{k T_{GS}} \right)^{1/\sqrt{n_*}}, 1 \right], \quad (12)$$

where  $\langle \zeta \rangle = \int_{s_h}^{s_w} p(s) ds + \int_{s_w}^{s^*} \frac{s - s_w}{s^* - s_w} p(s) ds$ , with integrals representing mean  $\zeta$  when soil saturation is below and above  $s_w$ , respectively, and assuming that  $\langle \zeta \rangle$  above  $s^*$  is zero;  $T_{GS}$  is mean growing season length (days);  $\langle T_* \rangle = \frac{P(s^*)}{\rho(s^*) p(s^*)}$ ;  $P(s)$  is the cumulative soil saturation probability density function;  $n_* = T_{GS} / T_*$ ; and  $k$  is an index that can be interpreted as the  $\langle \zeta \rangle$  a plant can experience during the duration  $T_{GS}$  without suffering from permanent damage (leading to  $\theta = 1$ ). In the absence of specific information, we prescribe a fixed value  $k = 2/3$ , which ensures that  $\theta < 1$  for all study sites.

This probabilistic formulation of plant water stress is heuristic, but translates complex links between soil water deficit and loss of photosynthesis, including both temporal and permanent physiological damage to provide a parsimonious but realistic measure of long-term cost of water stress for plant productivity and links to water use efficiency (Porporato et al., 2001).

### 2.2.3. Plant water use performance

We define plant water use performance ( $\varepsilon$ , unitless), as stress-weighted transpiration normalized by water availability (Bassiouni et al., 2020; Caylor et al., 2006)

$$\varepsilon = (1 - \langle \theta \rangle) \langle T \rangle / \langle P \rangle. \quad (13)$$

This metric of plant water use performance represents the tradeoff between water uptake, leading to carbon gains and growth (represented by  $\langle T \rangle / \langle P \rangle$ ), and risks of unfavorable water-stressed conditions, during which the water penalty of opening stomata to fix carbon is greater and leads to high costs of water use (represented by  $1 - \langle \theta \rangle$ ). In other words, long-term transpiration is linked to plant productivity through  $(1 - \langle \theta \rangle)$ , which is defined to capture long-term water use efficiency (Porporato et al., 2001). With this approach, water use performance is evaluated without directly estimating photosynthesis. Moreover, by quantifying performance relative to available water,  $\varepsilon$  is also a measure of water productivity, which is a meaningful measure for comparisons between ecosystems in different climates.

Next, we assume that plant traits adapt to maximize water use performance (Eq. (13)). This approach is similar to optimality criteria adopted in stomatal optimization theories (Mencuccini et al., 2019; Wang et al., 2020), but now using our minimalist ecohydrological framework. While there is no consensus on the most appropriate

formulations of optimality criteria and constraints for different spatial, temporal, or organization scales (Bassiouni and Vico, 2021; Sabot et al., 2022), leveraging dynamic plant water stress ( $\theta$ ) allows for the optimality formulation to account for cumulative impacts of soil moisture deficits on net carbon gain as opposed to typically assumed instantaneous performance maximization (Feng et al., 2022; Lu et al., 2020).

### 2.3. Framework application

We first explore the role of the  $\Pi$  groups theoretically using baseline parameter values for a temperate broadleaf forest (Table 1) as a sample ecosystem. We then apply the framework at 40 selected ecosystems using prescribed site-specific soil texture, vegetation structure, and climate parameters derived from data and metadata (Table S1) and inferring the four unknown plant traits ( $\psi_{g,50}$ ,  $\psi_{x,50}$ ,  $k_{x,max}$ ,  $RAI$ ) through model inversion to quantify associated  $\Pi$  groups and the shape parameters for  $\beta(s, \Pi)$ .

Rooting depth plays an integral role in defining plant water use strategies via both  $K_{SR, max}$  and the soil water balance. However, here we focus on variations of other eco-physiological traits and constrain  $Z$  to site-specific values consistent with available soil moisture data. Specifically, we prescribe  $Z$  as 1.5 times the soil moisture measurement depth (Table S1), which generally corresponds to the average rooting depth in the studied biomes. As such, we limit our analysis to  $\Pi$  groups in the eco-physiological model defining the shape of  $\beta(s, \Pi)$  (Section 2.1), rather than the ecohydrological model (Section 2.2).  $\Pi$  groups for the ecohydrological model have been previously defined and studied for the partitioning of the soil water balance (e.g. Feng et al., 2012; Porporato et al., 2004) as well as in the context of optimal  $Z$  across climatic gradients (Guswa, 2010), namely  $\frac{E_0}{\alpha \Delta}$  (the aridity index) and  $\frac{(s_{fc} - s_w)nz}{\alpha}$  (the soil water storage index).

#### 2.3.1. Data

We use daily observations and site characteristics from 40 sites (Table S1) in the FLUXNET2015 dataset (Pastorello et al., 2020) as well as satellite LAI estimates (Myneni et al., 2015). We select sites and

quality check records to best meet soil water balance model assumptions and only analyze growing season data – see Methods S1 and Table S1 for details about data and site selection. The model requires rainfall, net radiation, and air temperature climate data inputs. We evaluate model results against soil moisture observations as well as independent (not used in parameter inference) total evapotranspiration and gross primary productivity measured by eddy-covariance.

#### 2.3.2. Parameter inference and evaluation

For each site, we infer two sets of parameters with (i) a data-driven criterion, maximizing the goodness-of-fit between empirical (derived from data) and theoretical (Eq. (8)) soil saturation probability distributions,  $p(s)$ , and (ii) the ecohydrological optimality criterion, maximizing plant water use performance,  $\epsilon$  (Eq. (12)). We adapt a Bayesian inference algorithm from previous work (Bassiouni et al., 2020, 2018) to this study's improved soil water balance, which explicitly partitions evapotranspiration and is eco-physiologically constrained by plant traits represented in  $\Pi$  groups – see Methods S2 for details about parameter inference.

We compare parameter sets as well as metrics of plant water uptake capacity and water use performance emerging from both criteria and hypothesize that ecohydrological optimality explains plant water use strategies encoded in soil moisture observations. To evaluate the predictive skill of our modeling approach at each site, we calculate the theoretical  $p(s)$  applying both the data-driven and optimality-based parameter sets. We then quantify goodness-of-fit compared to the empirical  $p(s)$ , derived from soil moisture time series, using a quantile-level Nash-Sutcliffe efficiency ( $NSE = 1$  indicates a perfect model,  $NSE < 0$  indicates that the model has less predictive skill than mean  $s$ ). Previous studies using this metric considered  $NSE < 0$  unacceptable and  $NSE \geq 0.5$  a good match (Bassiouni et al., 2020, 2018). As an additional and independent measure of predictive skill, we compare optimality-based model results to record-averaged growing season total evapotranspiration and gross primary productivity across the selected 40 ecosystems.

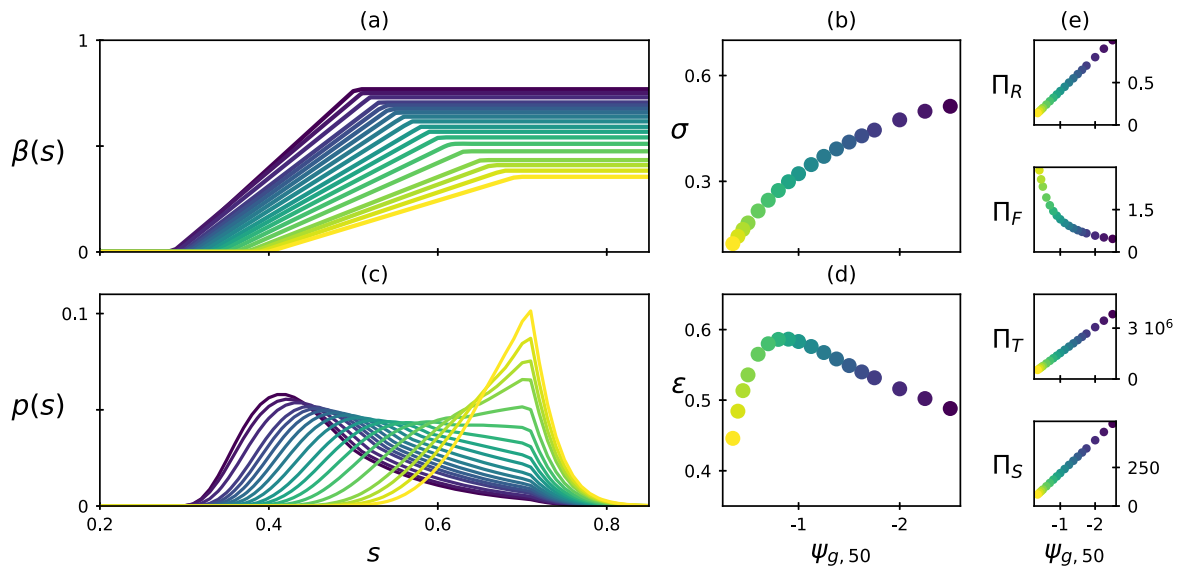


**Fig. 2.** Water use strategies with varying stomatal sensitivity represented by the water potential at 50% loss of stomatal conductance ( $\psi_{g,50}$ ). (a) Fraction of transpiration to potential atmospheric demand ( $\beta$ , Eq. (2)); (b) index of plant water uptake capacity ( $\sigma$ , Eq. (6)); (c) soil saturation probability density function ( $p(s)$ , Eq. (8)); (d) plant water use performance ( $\epsilon$ , Eq. (13)); (e) effect of  $\psi_{g,50}$  on non-dimensional groups: hydraulic risk tolerance ( $\Pi_R$ ), plant water flux control ( $\Pi_F$ ), soil-to-root water transport capacity ( $\Pi_T$ ), and soil suitability ( $\Pi_S$ ). Prescribed parameter values are for a temperate broadleaf forest with loam soil texture (Table 1).  $\psi_{g,50}$  ranges from  $-0.35$  (yellow) to  $-2.5$  (purple) MPa according to the color scale on the x-axis in subplots b, d, and e.

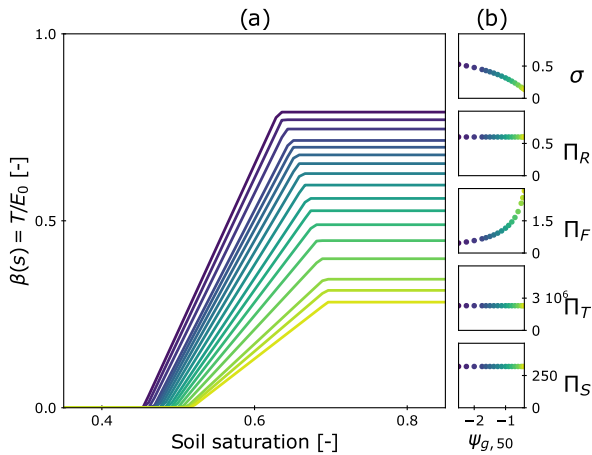


**Fig. 3.** Effect of plant water flux control ( $\Pi_F$ ) on (a) the fraction of transpiration ( $T$ ) to potential atmospheric demand ( $E_0$ ) as a function of soil saturation ( $\beta(s)$ , Eq. (2)), (b) plant water uptake capacity ( $\sigma$ , Eq. (6)) representing the normalized area of the  $\beta(s)$  function; and non-dimensional groups for hydraulic risk tolerance ( $\Pi_R$ ), plant water flux control ( $\Pi_F$ ), soil-to-root water transport capacity ( $\Pi_T$ ), and soil suitability ( $\Pi_S$ ). We obtain water use strategies for different values of  $\Pi_F$  by varying the water potential at 50% loss of stomatal conductance ( $\psi_{g,50}$ ) and maintaining other 3  $\Pi$  groups constant by adjusting  $\Pi_R$  with the water potential at 50% loss of xylem conductance ( $\psi_{x,50}$ ),  $\Pi_T$  with maximum soil-root conductance ( $K_{SR,max}$ ), and  $\Pi_S$  with soil water potential near saturation ( $\psi_{s,sat}$ ) to counterbalance the effect of varying  $\psi_{g,50}$ . Baseline parameter values are in Table 1.  $\psi_{g,50}$  ranges from  $-0.35$  (yellow) to  $-2.5$  (purple) MPa according to the color scale on the x-axis in subplots b.

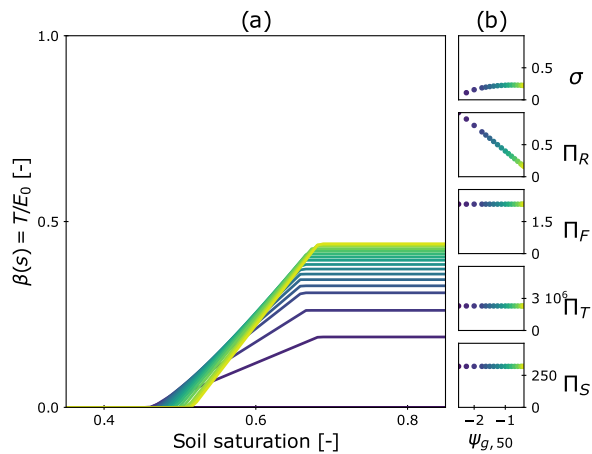


**Fig. 4.** Effect of hydraulic risk tolerance ( $\Pi_R$ ) on (a) the fraction of transpiration ( $T$ ) to potential atmospheric demand ( $E_0$ ) as a function of soil saturation ( $\beta(s)$ , Eq. (2)), (b) plant water uptake capacity ( $\sigma$ , Eq. (6)) representing the normalized area of the  $\beta(s)$  function; and non-dimensional groups for hydraulic risk tolerance ( $\Pi_R$ ), plant water flux control ( $\Pi_F$ ), soil-to-root water transport capacity ( $\Pi_T$ ), and soil suitability ( $\Pi_S$ ). We obtain water use strategies for different values of  $\Pi_R$  by varying the water potential at 50% loss of stomatal conductance ( $\psi_{g,50}$ ) and maintaining other 3  $\Pi$  groups constant by adjusting  $\Pi_F$  with maximum plant xylem conductance ( $K_{P,max}$ ),  $\Pi_T$  with maximum soil-root conductance ( $K_{SR,max}$ ), and  $\Pi_S$  with soil water potential near saturation ( $\psi_{s,sat}$ ) to counterbalance the effect of varying  $\psi_{g,50}$ . Baseline parameter values are in Table 1, except we divide maximum xylem conductance by 3 to exaggerate the range of  $\beta(s)$  patterns.  $\psi_{g,50}$  ranges from  $-0.35$  (yellow) to  $-2.5$  (purple) MPa according to the color scale on the x-axis in subplots b.

### 3. Results

#### 3.1. Plant water flux control is the primary axis of variation in water use strategies

Plant traits, individually, alter  $\Pi$  groups and consequently plant water use strategies reflected in the shape of  $\beta(s, \Pi)$ . However, multiple combinations of individual traits can produce  $\Pi$  groups of the same value and therefore lead to the same behavior in terms of plant water uptake capacity ( $f_{ww}$ ,  $s^*$ ,  $s_w$ , and  $\sigma$ , Eqs. (3)-(6) and same ecohydrological outcomes in terms of plant water use performance ( $\epsilon$ , Eq. (13)). Further, combinations of different  $\Pi$  groups can also lead to similar results because  $\Pi$  groups interact (Eqs. (4) and (5)) to determine water flux through the SPAC reflected in the shape of  $\beta(s, \Pi)$ . Plant water flux control ( $\Pi_F$ ) and hydraulic risk tolerance ( $\Pi_R$ ) affect all three  $\beta(s, \Pi)$  shape parameters, while soil suitability ( $\Pi_S$ ) and soil-root water transport capacity ( $\Pi_T$ ) only affect  $s^*$  and  $s_w$  and do not influence  $f_{ww}$  Eqs. (4) and (5). We summarize and illustrate the role of the  $\Pi$  groups theoretically (Figs. 2-5 and Figs. S2 – S5) varying baseline parameter values (Table 1).

Stomatal sensitivity,  $\psi_{g,50}$ , affects  $f_{ww}$ ,  $s^*$ ,  $s_w$ , and hence the shape of  $\beta(s, \Pi)$  (Fig. 2a), through its appearance in all four  $\Pi$  groups (Fig. 2e). With more sensitive stomatal control (less negative  $\psi_{g,50}$ ) and all else being equal,  $f_{ww}$  decreases and  $s^*$  and  $s_w$  increase towards wetter states. Consequently, the overall index of plant water uptake capacity decreases, leading to increasingly stress-averse strategies (decreasing  $\sigma$ ;

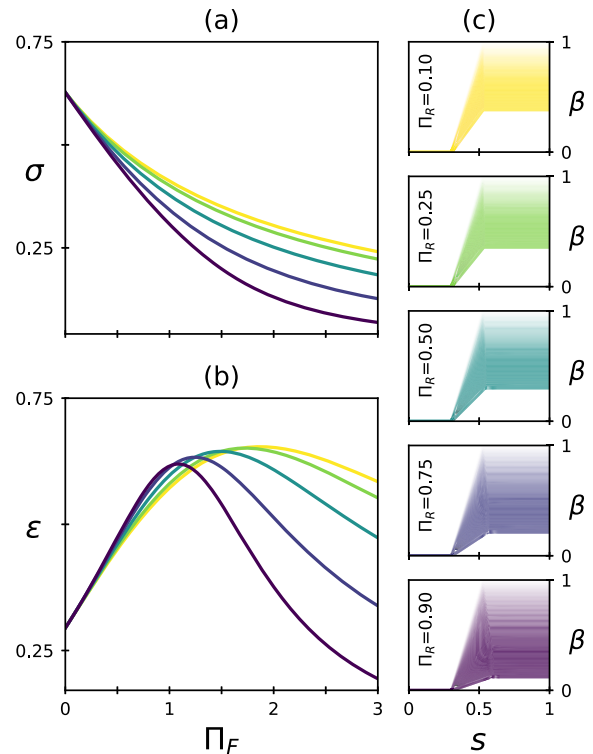


**Fig. 5.** Effect of plant water flux control ( $\Pi_F$ ) and hydraulic risk tolerance ( $\Pi_R$ ) with constant water potential at 50% loss of stomatal conductance ( $\psi_{g,50}$ ) on (a) index of plant water uptake capacity ( $\sigma$ , Eq. (6)); (b) plant water use performance ( $\epsilon$ , Eq. (13)); (c) fraction of transpiration to potential atmospheric demand ( $\beta$ , Eq. (2)) as a function of soil saturation ( $s$ ), when varying  $\Pi_R$  (increasing from top (yellow,  $\Pi_R = 0.10$ ) to bottom (purple,  $\Pi_R = 0.90$ )) and  $\Pi_F$  (increasing from darker ( $\Pi_F \approx 0$ ) to lighter ( $\Pi_F = 3$ ) colors in each sub-panel). Prescribed baseline parameter values are for a temperate broadleaf forest with loam soil texture (Table 1) and varying maximum plant conductivity ( $K_{p,max}$ ) and water potential at 50% loss of xylem conductance ( $\psi_{x,50}$ ) to change  $\Pi_F$  and  $\Pi_R$ , respectively.

moving from purple to yellow curves in Fig. 2b). With decreasing  $\sigma$  and progressively downregulated transpiration, soil saturation probability distributions,  $p(s)$ , shift to wetter states because plants conserve more water (Fig. 2c). Additionally, plant water use performance,  $\varepsilon$ , increases to a maximum and then declines as stomatal sensitivity increases (Fig. 2d) because stress-tolerant plants (very negative  $\psi_{g,50}$ ) are more likely to be water stressed due to less constrained and excessive water use, while overly conservative strategies do not use available water effectively.

The other key SPAC variables can counterbalance effects of  $\psi_{g,50}$  in each individual  $\Pi$  group, leading to combinations of  $\Pi$  groups that determine a wider spectrum of water uptake capacity than those exemplified in Fig. 2. Variables that interact with  $\psi_{g,50}$  include xylem vulnerability ( $\psi_{x,50}$ ) in  $\Pi_R$ ; plant size and hydraulic architecture that define  $K_{P,max}$  ( $LAI$ ,  $h_c$ ,  $k_x$ ,  $max$ ) in  $\Pi_F$ ; soil and root properties that define  $K_{SR,max}$  ( $k_{s,sat}$ ,  $RAD$ ) in  $\Pi_T$ ; and soil water holding capacity ( $\psi_{s, sat}$ ) in  $\Pi_S$ . However, the extent to which water use strategies deviate from the general pattern imposed by  $\psi_{g,50}$  alone (Fig. 2) is constrained by ranges of trait values documented in different biomes (e.g. Manzoni et al., 2013a). Certain combinations of  $\Pi$  groups (and water use strategies) can result from a large diversity of co-existing traits, while other strategies can only occur for more specific trait combinations due to constraints of atmospheric water demand ( $E_0$ ) and soil texture. While soil and root properties can influence the shape of  $\beta(s, \Pi)$ , we conclude that they do not considerably counterbalance effects of aboveground plant traits. This is because differences in soil texture and root area index (summarized in  $\Pi_S$  and  $\Pi_T$ ) result into negligible variations in relative plant water uptake capacity (Fig. S2 – S5). Note that here we explore relative plant water uptake capacity for a given rooting zone, to isolate from the strong controls of soil texture and rooting depth on available soil water through interacting with the total water balance.

Decreasing plant water flux control and all else being equal (decreasing  $\Pi_F$ ; moving from yellow to purple curves in Fig. 3) results in more stress-tolerant strategies (increasing  $\sigma$ ) by both increasing  $f_{ww}$ , which enhances water uptake in wetter states, and decreasing  $s^*$  and  $s_w$ , which increases water uptake in dry states. For set plant traits,  $\Pi_F$  decreases when atmospheric water demand ( $E_0$ ) decreases. As a result of lower  $E_0$ , plant water transport becomes less limiting and  $\sigma$  accordingly increases. Increasing plant hydraulic risk tolerance and all else being equal (increasing  $\Pi_R$ , Fig. 4) decreases  $s^*$  and  $s_w$ , as well as  $f_{ww}$ , which leads to more conservative water uptake at wetter states and little change to  $\sigma$  compared to decreasing  $\Pi_F$ .

Hydraulic risk tolerance ( $\Pi_R$ ) modulates the effect of plant water flux control because  $\Pi_R$  influences the sensitivity of the relation between  $\Pi_F$  and  $\sigma$  (Fig. 5). For a fixed  $\psi_{g,50}$  but varying  $\psi_{x,50}$  and  $K_{P,max}$ , the capacity to take up soil water decreases more steeply with increasing  $\Pi_F$  at high compared to low  $\Pi_R$  (moving from purple to yellow curves in Fig. 5a). Because increasing  $\Pi_F$  also lowers water stress, plant water use performance,  $\varepsilon$ , peaks at intermediate values of  $\Pi_F$ , and the  $\Pi_F$  value at the peak increases with decreasing  $\Pi_R$  (Fig. 5a). This means that at low  $\Pi_F$ , the value of  $\Pi_R$  has little effect on water use performance, and that the combination of both high  $\Pi_F$  and  $\Pi_R$  leads to lowest performance. High risk tolerance is thus not beneficial in combination with high plant limitations on water flux (low  $K_{P,max}|\psi_{g,50}|$  increases  $\Pi_F$ ) or high atmospheric water demand (high  $E_0$  increases  $\Pi_F$ ).

In summary, plant water use strategies represented by the shape of  $\beta(s, \Pi)$  are primarily defined by plant water flux control ( $\Pi_F$ ), therefore also influencing plant water uptake capacity and water use performance as well as their sensitivity to climate variability. Plant hydraulic risk tolerance ( $\Pi_R$ ) has a smaller influence and interacts with water flux control especially when plant water transport is limiting (high  $\Pi_F$ ). Risk aversion versus tolerance (low to high  $\Pi_R$ ) only affects water use performance when atmospheric water demand is much greater than plant water transport capacity (higher values of  $\Pi_F$ ) and depends directly on climate in the definition of  $\Pi_F$  and indirectly on the timing and amount

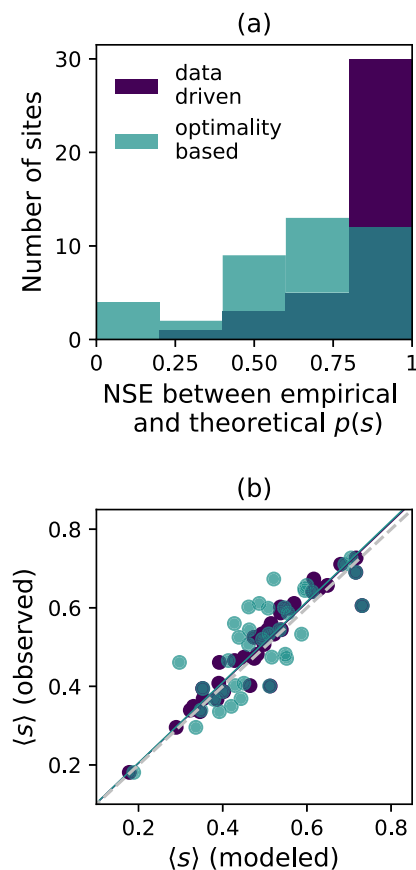


**Fig. 6.** Predictive skill of the parameterized soil water balance. (a) Distribution of the goodness-of-fit in terms of the Nash-Sutcliffe efficiency (NSE) between empirical and theoretical soil saturation probability distributions using parameters inferred from the data-driven criterion (purple) and the optimality criterion (blue). Areas where histograms overlap appear in dark blue. (b) Correlation between long-term average growing season observed and modeled soil saturation using data-driven ( $r = 0.95$ ,  $RMSE = 0.04$ ,  $bias = -2.5\%$ ) and optimality-based ( $r = 0.83$ ,  $RMSE = 0.07$ ,  $bias = -3.2\%$ ) parameter estimates. Pearson's correlation coefficients ( $r$ ) are statistically significant with  $>99\%$  confidence. Solid colored lines in (b) represent the regression fit through the origin. Gray dashed line in (b) indicates the 1:1 line.

of rainfall interacting with  $\Pi_F$  via  $\beta(s, \Pi)$  in the water balance. Importantly, the theoretical patterns suggest an optimal range of traits that maximize plant water use performance and not all possible combinations of plant traits and  $\Pi$  groups may be viable depending on the degree of climate variability.

### 3.2. Optimal water use strategies maximize long-term mean transpiration weighted by risks of water stress

Building on the theoretical results, we apply our framework across the selected 40 ecosystems to test the ecohydrological optimality criterion (maximizing Eq. (13)). The median Nash-Sutcliffe efficiency (NSE) between empirical and the theoretical soil saturation probability distributions,  $p(s)$ , is 0.9 using parameters that maximize the fit with soil moisture observations (data driven criterion) and 0.7 using parameters that maximize plant water use performance  $\varepsilon$  (optimality criterion) (Fig. 6a). Applying the model using the data-driven and optimality-based parameters explains 95 and 83%, respectively, of the variability in long-term mean growing season soil saturation observed across the 40 ecosystems (Fig. 6b). Therefore, comparing predictive model skill using the optimality criterion (with independent theoretically estimated parameters) and the data-driven criterion (with empirically fitted parameters) lends support to our parsimonious approach.

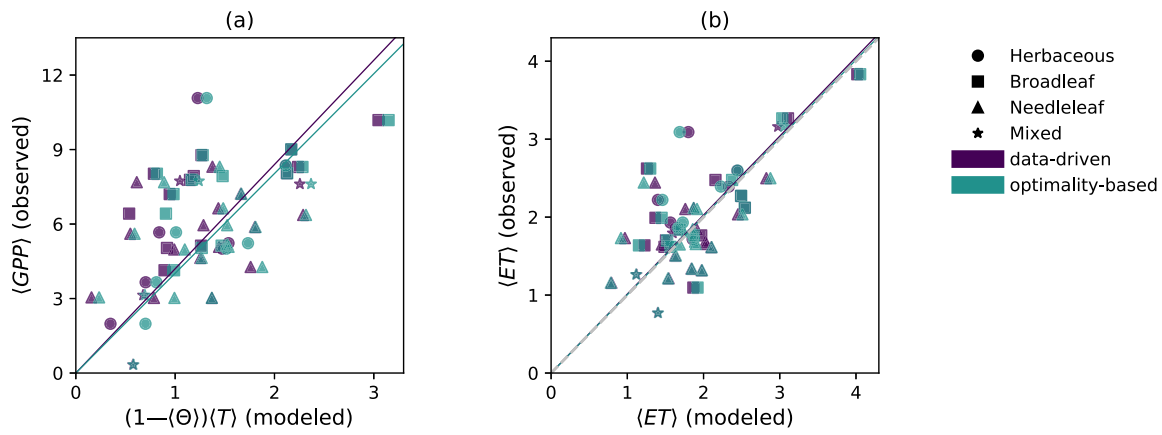


**Fig. 7.** Modeled and observed ecohydrological fluxes. (a) Correlation between long-term average growing season observed gross primary productivity ( $\langle GPP \rangle$ ,  $\text{gC m}^{-2} \text{d}^{-1}$ ) and modeled stress-weighted transpiration ( $(1 - \langle \theta \rangle) \langle T \rangle$ ,  $\text{mm d}^{-1}$ ) using data-driven ( $r = 0.54$ ) and optimality-based ( $r = 0.55$ ) parameter sets for 40 ecosystems (Table S1). (b) Correlation between observed long-term average growing season modeled versus observed total evapotranspiration ( $\langle ET \rangle$ ,  $\text{mm day}^{-1}$ ) for data driven ( $r = 0.68$ ,  $\text{RMSE} = 0.51$ ,  $\text{bias} = -4.6\%$ ) and optimality-based ( $r = 0.67$ ,  $\text{RMSE} = 0.51$ ,  $\text{bias} = -3.9\%$ ) parameter sets. Pearson's correlation coefficients ( $r$ ) are statistically significant with  $>99\%$  confidence. Markers indicate dominant plant functional types at each site. Mixed ecosystems include temperate and boreal forests with mixture of broadleaf and needleleaf trees as well as tropical and Mediterranean savannas and shrublands with a mixture of herbaceous and woody vegetation. Solid colored lines represent the regression fit through the origin and gray dashed line in (b) indicates the 1:1 line.

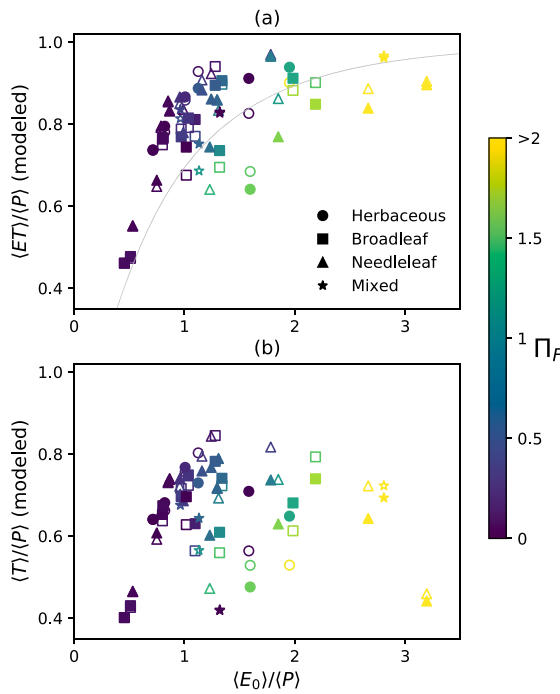


**Fig. 8.** Model partitioning of long-term average growing season rainfall ( $\langle P \rangle$ ) into (a) total evaporation ( $\langle ET \rangle$ ) and (b) only transpiration ( $\langle T \rangle$ ) as a function of aridity measured by the ratio between long-term average growing season potential evaporation ( $\langle E_0 \rangle$ ) and  $\langle P \rangle$  for 40 ecosystems (Table S1), using the data-driven (open markers) and optimality-based (solid markers) parameter sets. Colors indicate plant water flux control ( $\Pi_F$ ). The gray line in (a) represents the average global annual water balance tendency (Budyko, 1974) as  $\sqrt{\langle E_0 \rangle / \langle P \rangle} (1 - e^{-\langle E_0 \rangle / \langle P \rangle}) \tanh(\langle P \rangle / \langle E_0 \rangle)$ . Markers indicate dominant plant functional types at each site. Mixed ecosystems include temperate and boreal forests with mixture of broadleaf and needleleaf trees as well as tropical and Mediterranean savannas and shrublands with a mixture of herbaceous and woody vegetation.

The posed metric of stress-weighted transpiration ( $\epsilon$ , Eq. (13)) using optimality-based parameters also explained 55% of the variability in long-term average growing season gross primary productivity across the 40 ecosystems (Fig. 7a). Further, the ecohydrological model using

optimality-based parameters explains 67% of the variability in long-term average growing season total evapotranspiration (Fig. 7b) and reproduces patterns in long-term water balance partitioning along the aridity axis (Fig. 8a) as well as a mesic maximum in the transpiration fraction (Fig. 8b), consistent with other empirical and modeling studies (Budyko, 1974; Good et al., 2017; Paschalis et al., 2018; Porporato et al., 2004).

Our comparison of data-driven and optimality-based parameter estimates (Fig. 9) indicates that the shape of  $\beta(s)$  that best captures observed soil moisture variability is also ecohydrologically optimal in terms of maximizing water use performance ( $\epsilon$ , Eq. (13)). Pearson's correlations between data-driven and optimality-based parameter estimates range from  $>0.9$  for  $f_{ww}$ ,  $s_w$ , and  $\Pi_F$ , to 0.41 for  $\Pi_R$ . The biases between data-driven and optimality-based parameter estimates range from  $<5\%$  for  $f_{ww}$  and  $\Pi_F$ , to 32% for  $\Pi_R$  (Fig. 9). The high correlations and low bias between data-driven and optimality-based estimates suggest that the shape of  $\beta(s)$  is well constrained, despite some uncertainty regarding specific nuances in plant water use strategies. For example, the degree of plant hydraulic risk ( $\Pi_R$ ) is not critical to define daily plant water uptake capacity in most biomes. Our findings therefore support the hypothesis that plant traits are adapted to growing season environmental conditions and maximize water use performance in terms of balancing long-term mean transpiration and risks of water stress ( $\epsilon$ , Eq. (13)).

The root-mean-square difference between water use performance,  $\epsilon$ , resulting from the best-fit models and maximum  $\epsilon$  from the optimality-based models is 0.08, and the bias indicates that ecosystems, as characterized by soil moisture observations, are on average within 9% of their maximum theoretical water use performance. Water use performance based only on static stress ( $\zeta$ ) leads to much greater differences between data-driven and optimality-based parameters and a bias towards more stress-tolerant strategies (Fig. S6). This demonstrates the importance of using of dynamic stress ( $\theta$ ) when defining water use performance and the need to account for the number and duration of periods with soil saturation below the threshold  $s^*$  during the growing season. The comparison between  $\zeta$  and  $\langle \theta \rangle$  also underlines that both the amount and timing of rainfall affect the long-term cost of water use due to cumulative stress.

Despite the coordination expected between water flux control ( $\Pi_F$ ) and hydraulic risk tolerance ( $\Pi_R$ ) given their dependence on stomatal sensitivity ( $\psi_{g,50}$ ) in the analytical model, Pearson's correlation between optimal  $\Pi_F$  and  $\Pi_R$  values is weak (Fig. S7,  $r = -0.1$ ). This means that

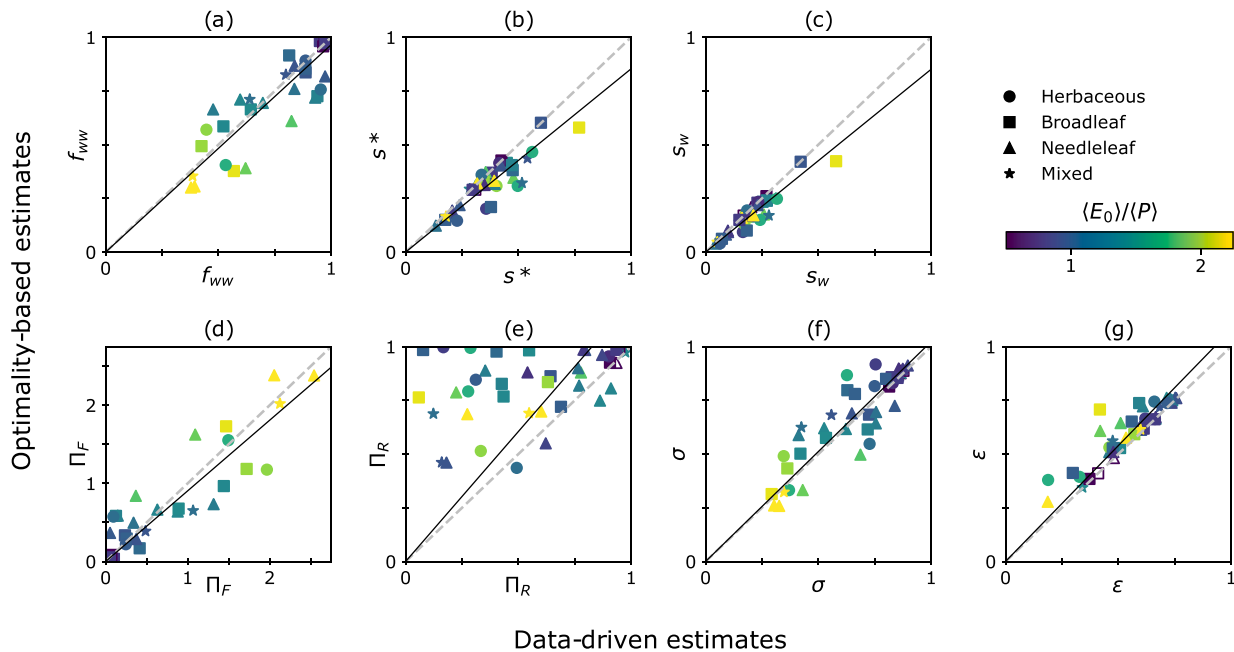


**Fig. 9.** Relation between data-driven water use strategies that maximize the goodness-of-fit between empirical and theoretical  $p(s)$  and optimality-based estimates that maximize plant water use performance using data from 40 study sites (Table S1). (a) Fractional loss of conductance in well-watered conditions ( $f_{ww}$ ,  $r = 0.90$ , RMSD = 0.10, bias = -3.4%); (b) soil saturation at the point of incipient stomatal closure ( $s^*$ ,  $r = 0.87$ , RMSD = 0.08, bias = -15.4%); (c) soil saturation at the wilting point ( $s_w$ ,  $r = 0.93$ , RMSD = 0.05, bias = -15.3%); (d) plant water transport control ( $\Pi_F$ ,  $r = 0.92$ , RMSD = 0.29, bias = -1.7%); (e) plant hydraulic risk tolerance ( $\Pi_R$ ,  $r = 0.41$ , RMSD = 0.37, bias = 31.7%); (f) overall index of plant water uptake capacity ( $\sigma$ ,  $r = 0.88$ , RMSD = 0.10, bias = 3.3%); (g) plant water use performance ( $\epsilon$ ,  $r = 0.91$ , RMSD = 0.08, bias = -9.0%). Pearson’s correlation coefficients ( $r$ ) are statistically significant with >99% confidence. Markers indicate dominant plant functional types at each site. Mixed ecosystems include temperate and boreal forests with mixture of broadleaf and needleleaf trees as well as tropical and Mediterranean savannas and shrublands with a mixture of herbaceous and woody vegetation. Color indicates growing season aridity, measured by the ratio between long-term average potential evaporation ( $E_0$ ) and rainfall ( $P$ ). Markers with empty face colors distinguish sites with poor goodness of fit (NSE < 0) between the theoretical and empirical  $p(s)$  using the optimality-based parameter estimates (2 out of 40). Gray dashed lines indicate the 1:1 lines.

**Table 3**

Correlations between water use strategies and climate parameters. Values indicate the Pearson’s correlation coefficient for data-driven (and optimality based) parameter estimates with at least 95% confidence and ‘ns’ indicate non-significant correlations. Index of plant water uptake capacity ( $\sigma$ ), plant water transport control ( $\Pi_F$ ), and plant hydraulic risk tolerance ( $\Pi_R$ ), aridity index ( $E_0/P$ ), long-term average atmospheric water demand ( $E_0$ ), rainfall intensity ( $\alpha$ ), rainfall frequency ( $\lambda$ ), long-term average precipitation ( $P = \alpha \lambda$ ).

	$\langle E_0/P \rangle$	$\langle E_0 \rangle$	$\sigma$	$\lambda$
$\sigma$	-0.80 (-0.85)	-0.39 (-0.44)	0.37 (0.35)	ns (ns)
$\Pi_F$	0.86 (0.92)	0.32 (0.36)	ns (ns)	-0.35 (-0.38)
$\Pi_R$	-0.35 (-0.33)	ns (-0.37)	0.31 (0.33)	ns (ns)

these two  $\Pi$  groups can be useful targets for parameter inference and represent two complementary aspects of water use strategies. However,  $\Pi_R$  is more difficult to infer from data especially in humid conditions and the goodness-of-fit between data-driven and optimality based  $\Pi_R$  was poor (Fig. 9e). This is expected from the model theoretical behavior (Fig. 5) showing that plant risk tolerance, summarized by  $\Pi_R$ , has a minor effect on plant water uptake capacity and performance when atmospheric water demand is lower than plant water transport capacity (low  $\Pi_F$ ) and the negative correlation confirms that having both high  $\Pi_F$  and high  $\Pi_R$  is not ecohydrologically successful. The inference algorithm converges to robust estimates of the lumped parameters ( $f_{ww}$ ,  $s^*$ ,  $s_w$ ) despite higher uncertainty in estimates of individual traits (mean coefficient of variation of posteriori parameter estimates <0.05 versus between 0.1 and 1). Therefore, lumped parameters and  $\Pi$  groups describing the SPAC, rather than individual traits, provide a more constrained and robust definition of  $\beta(s, \Pi)$  and the associated ecohydrological functions at the ecosystem level.

The water use strategies emerging from the optimal  $\Pi$  group values do not vary consistently between plant functional types. Under the same growing season conditions, both needle leaf forests and grasslands can have the same  $\Pi$  group values, resulting from different possible trait combinations. The variability in water use strategies are primarily explained by aridity ( $\langle E_0/P \rangle$ , Fig. 9). For example, the most stress-avoidant strategies (high  $\Pi_F$ , low  $\Pi_R$ , low  $\sigma$ ) are found in Mediterranean climates including needleleaf, broadleaf, and savanna ecosystems. Statistically significant correlation coefficients between ( $E_0/P$ ) and  $\sigma$ ,  $\Pi_F$ , and  $\Pi_R$  are -0.80 (-0.85), 0.86 (0.92), and -0.35 (-0.33), respectively, for data-driven (and optimality-based) estimates (Table 3). However,  $\sigma$  is more correlated with  $E_0$  than rainfall characteristics;  $\Pi_F$  is more correlated with rainfall frequency; and  $\Pi_R$  is more correlated with rainfall intensity (Table 3).

#### 4. Discussion

We analyze soil moisture observations, a key ecosystem variable, to evaluate whether plants achieve efficient soil water use by coordinating SPAC biotic components, as previously hypothesized (Manzoni et al., 2013b; Mencuccini et al., 2015; Prentice et al., 2014; Reich, 2014). We seek to improve understanding of ecosystem-climate interactions beyond previous studies that explain variations in individual plant functional traits with average long-term climate characteristics such as mean annual precipitation and temperature (Choat et al., 2012), as well as improve empirical quantification of variability in ecosystem-scale water stress responses with uncertain eco-physiological underpinnings (Bassiouni et al., 2020; Fu et al., 2022; Yanlan Liu et al., 2021). We therefore take a holistic view and explain variations in plant water use strategies using non-dimensional  $\Pi$  groups within an ecohydrological model. This framework combines plant traits, soil and climatic

conditions to link strategies to a dynamic metric of plant water use performance that accounts for feedbacks due to risk of plant water stress (Figs. 2–5). We find that individual traits do not determine optimal plant water use strategies and water use performance because various combinations of trait values lead to similar ecohydrological outcomes. Importantly, parameters defining plant water use strategies that maximize water use performance also capture temporal variability in soil moisture within ecosystems ( $p(s)$ ) and spatial variability in long-term growing season ecohydrological fluxes across wet to arid ecosystems (Figs. 6–7). The ecohydrologically optimal plant water use strategies point to coordination in plant traits to meet atmospheric water demand and stochastic water availability that influence stress risk and cumulative drought impacts. Despite its parsimony, this tractable quantification of plant water use strategies and ecohydrological performance offers promising avenues to parameterize and diagnose plant responses to water limitations under climate change. Further, alternative optimality and coordination hypotheses can be tested by revisiting our framework with different or more complex performance criteria and  $\Pi$  groups incorporating additional processes and tradeoffs.

#### 4.1. Ecohydrological coordination, reflected in $\Pi$ groups, simplifies the description of plant water uptake

Non-dimensional  $\Pi$  groups, summarizing key eco-physiological tradeoffs, capture simultaneously biotic and abiotic controls on plant water use strategies in a tractable model, leading to an effective but parsimonious description of ecosystem-climate interactions. We focus on the shape of the relation between soil moisture and transpiration relative to potential atmospheric water demand ( $\beta(s, \Pi)$ ) and identify non-dimensional axes of variation that are not directly apparent when looking at individual traits due to covariations among plant traits and environmental conditions in which plants grow. The dominant axis capturing variations in water use strategies is the plant water flux control ( $\Pi_F$ ), which represents the ratio of atmospheric water demand over plant-controlled water supply to the leaves. The dominance of  $\Pi_F$  points to the importance of combined climatic and plant characteristics in defining plant water use strategy. The plant risk tolerance axis ( $\Pi_R$ ), capturing coordination of hydraulic and stomatal traits within a plant and contrasting stomatal versus xylem sensitivity to water status, becomes influential when plant water transport is most limiting (high  $\Pi_F$ ). In other words,  $\Pi_F$  mainly drives variability in plant water uptake capacity ( $\sigma$ ) and  $\Pi_R$  regulates nuances in the sensitivity of  $\sigma$  to variability in  $\Pi_F$  due to changes in atmospheric water demand ( $E_0$ ) or plant size and hydraulic architecture ( $K_{p,max}$ ). The groups describing soil suitability ( $\Pi_S$ ) and soil-root transport capacity ( $\Pi_T$ ) were less influential. For a given rooting depth, they had no effect on soil water uptake in well-watered conditions ( $f_{ww}$ ) and only negligible impact on thresholds of soil water uptake ( $s_w$  and  $s^*$ ).

We demonstrate that  $\Pi$  groups explain stress responses in a wide range of ecosystems, thus expanding on a previous dimensional analysis of plant drought responses (Feng et al., 2018) and taking the concept a step further by incorporating  $\Pi$  groups in a modeling framework to improve understanding of the influence of plant traits in ecosystem-climate interactions. The two most influential axes, represented by  $\Pi_F$  and  $\Pi_R$ , are consistent with the ‘fast-slow’ plant economics spectrum (Reich, 2014). Slow trait strategies are associated with stress-avoidance due to limited plant water transport (high  $\Pi_F$ ) and/or risk avoidance (low  $\Pi_R$ ). However,  $\Pi_F$  combines eco-physiological and climatic variables, leading to a generalized and more meaningful approach for capturing variations at ecosystem levels compared to existing metrics for water use strategies based solely on traits (Skelton et al., 2015).  $\Pi_F$  is also related to sources of variation of previously identified major axes of ecosystem function, in particular water use efficiency, derived from exploratory data analyses (Díaz et al., 2016; Migliavacca et al., 2021). The added benefit is that  $\Pi$  groups have stronger mechanistic underpinnings and lead to a more transferrable

and generalizable approach.

Furthermore,  $\Pi$  groups combine different traits and reveal their coordination. A single  $\Pi$  group value can represent a wide range of possible individual traits characterizing a diversity of co-existing species in an ecosystem that lead to similar long-term water use performance. The relation between water balance and  $\Pi$  groups, rather than single parameters, has a practical implication because we show that calibrating traits in SPAC models will inevitably lead to multiple solutions. Our approach thus provides new avenues to reduce the complexity of quantifying ecosystem function and to increase model robustness (Prentice et al., 2015) by focusing on  $\Pi$  groups that embed ecologically meaningful mechanisms instead of individual parameters.

#### 4.2. Ecohydrological optimality explains plant water use strategies

Beyond summarizing the SPAC in a small number of non-dimensional groups, our parsimonious approach predicts ecologically successful water use strategies (optimality-based estimates) that are consistent with the long-term water balance spanning wet to arid climates (data-driven estimates) (Fig. 9). As such, this approach links and generalizes previous data-driven (Bassiouni et al., 2020) and theoretical studies (Feng et al., 2018; Manzoni et al., 2014). Optimal combinations of  $\Pi$  groups defining  $\beta(s)$  explain observed soil moisture variability ( $p(s)$ ) and encode combinations of plant traits that are most effective at using limited water resources accounting for the cost of water stress, as captured by the water use performance  $\epsilon$ . This implies that, at the ecosystem level, plants are adapted to growing season conditions to maximize water use performance. As a result, our framework provides a method to understand and parameterize the sensitivity of transpiration to soil moisture and potential atmospheric demand based on few easily available environmental variables, instead of prescribing or calibrating optimality costs or parameters as commonly done when modeling stomatal conductance (Mencuccini et al., 2019).

Aridity primarily influences optimal water use strategies, although these strategies vary among studied ecosystems and within plant functional types. Generally, variability in metrics of plant water uptake capacity ( $f_{ww}$ ,  $s^*$ ,  $s_w$ , and  $\sigma$ ) across biome and along the aridity axis are consistent with patterns and findings from previous empirical studies (Bassiouni et al., 2020; Fu et al., 2022). Further, the theoretical framework optimal  $\Pi_F$  significantly increases with decreasing rainfall frequency (water demand becomes more important during the longer dry spells), while optimal  $\Pi_R$  increases with increasing rainfall intensity (water stress is more ‘acceptable’ in wetter climates). Our findings indicate that both the timing and amount of rainfall are key to quantify risks of water stress and resulting water use performance. Importantly, the improved match between data-driven and optimality-based parameters using the dynamic water stress ( $\theta$ ) (Fig. 9) versus static water stress ( $\zeta$ ) (Fig. S6) points to long-term eco-evolutionary adaptation to stochastic water availability that influences the long-term cost of water use and the need to avoid both temporal and irreversible impacts on productivity. Our results therefore provide novel evidence that optimality inferred from long-term risks, rather than instantaneous impacts (Feng et al., 2022; Lu et al., 2020), is more consistent with ecohydrological data.

While most parameters estimated from the data- and theory-based approaches are very well correlated, the correlations for  $\Pi_R$  are poor (Fig. 9e). This does not necessarily undermine the validity of the ecohydrological optimality criteria and the importance of accounting for risks of water stress to quantify plant water uptake capacity and its sensitivity to environmental conditions. Rather, it points to some limitations of the long-term water balance framework and daily data in being able to disentangle the complexity of plant hydraulic risk tolerance, especially in humid environments.

Optimal water use strategies explain fundamental patterns of rainfall partitioning into evapotranspiration and percolation or runoff, and how the water balance is linked to plant drought responses ranging from

stress-tolerant to stress-averse (Fig. 8). Furthermore, transpiration weighted by water stress risks captures spatial variability in gross primary productivity and, despite its parsimony, proves a useful performance metric contrasting costs and benefits of water uptake under a wide variety of soil and climatic conditions (Fig. 7a). Our optimality criteria to identify  $\Pi$  groups complements previous ecohydrological models under stochastic rainfall and findings inferring grass-tree distributions (Caylor et al., 2006), optimal rooting depths (Guswa, 2010, 2008), coordination of stomatal and xylem vulnerability (Manzoni et al., 2014), and stomatal responses (Lu et al., 2016). Different from approaches optimizing single traits, quantifying  $\Pi$  groups provides a more holistic view of eco-evolutionary outcomes that accounts for expected co-variations across plant organs and between traits and the environment. Furthermore, while our framework is focused here on water use strategies in terms of the shape of  $\beta(s)$ , it can be extended to also assess optimal rooting depths and further improve the inference of tradeoffs between eco-physiological traits, rooting strategies, and vegetation distribution from ecosystem-scale data (Yaling Liu et al., 2021; Stocker et al., 2023) that emerge as adaptations to water availability.

Given known long-term climate characteristics,  $\Pi$  groups summarize ranges of possible trait combinations that can achieve similar functions and co-exist in an ecosystem. The framework offers further avenues to assess the evolutionary stability of resulting water use strategies. Therefore,  $\Pi$  groups can be useful to explain relations between trait diversity and local water availability (Trugman et al., 2020). The proposed optimality-based inference of water use strategies provides opportunities to investigate broad spatial patterns of optimal  $\Pi$  groups, how they relate to distributions of global ecosystems and potential vulnerability or adaptation to climate change, especially in ecosystems most vulnerable to increased water limitations.

#### 4.3. Tractable quantification of plant water use strategies

Leveraging dimensional analysis and optimality theory, we address the need for parsimonious and more transferable descriptions of water use strategies to bridge the gap between top-down data-driven approaches and bottom-up trait-based approaches. Scaling and aggregating individual plant traits to describe ecosystem-level transpiration with a bottom-up approach is complex and uncertain because tissue-level traits have nonlinear dependencies on plant size, and ecological performance and survival mechanisms shape community composition (Enquist et al., 2015; Mencuccini et al., 2019). Indirect inference approaches, using flux tower and satellite data, extend the representation of ecohydrological processes beyond plant-level measurements and provide ecosystem-scale parameters defining water use strategies globally (Bassiouni et al., 2020; Dralle et al., 2020; Fu et al., 2022; Konings and Gentine, 2017; Liu et al., 2020; Yaling Liu et al., 2021; Yanlan Liu et al., 2021; Stocker et al., 2023). However, results from inverse modeling can be conflated by their many assumptions and are still constrained by the coverage, uncertainty and quality of numerous data inputs. We therefore take a step forward and propose a complementary dimensionless optimality framework to infer water use strategies using minimal but realistic assumptions grounded in eco-physiological theory and requiring few readily available parameters (soil texture, mean growing season atmospheric water demand, rainfall characteristics, and leaf area index).

Non-dimensional  $\Pi$  groups summarize water use strategies by collapsing variability in traits into a minimal number of parameters, reducing the complexity of representing detailed SPAC hydraulics at the ecosystem level. Two non-dimensional groups (plant water flux control  $\Pi_F$  and hydraulic risk tolerance  $\Pi_R$ ) are key in determining the functional relation between transpiration, soil moisture and atmospheric water demand. This relation,  $\beta(s, \Pi)$ , uniquely determines our metrics of plant water uptake capacity ( $f_{wvs}$ ,  $s^*$ ,  $s_{wi}$ , and  $\sigma$ ). Therefore, despite uncertainty in individual trait estimates, metrics of plant water uptake capacity are well constrained, robustly estimated, and accurately

describe water use strategies adapted to the given soil and climate. The simplified eco-physiological model explains key ecological information encoded in hydrological observations and complements the data-driven approach.

Parametrizing existing empirical relations such as  $\beta(s, \Pi)$  using optimality principles and  $\Pi$  groups offers a promising avenue for next-generation models to incorporate ecological mechanisms and principles of community ecology (Harrison et al., 2021; Scheiter et al., 2013) without sacrificing model robustness or increasing complexity (as advocated by Prentice et al. (2015)). Ecosystem-scale relations between transpiration and soil moisture can potentially preserve their practical and parsimonious forms while approaching predictive capacity of full hydraulic models (Sloan et al., 2021). Optimality-based approaches, such as the one proposed here, can also provide useful constraints to reduce the uncertainty and enhance the interpretation of future data-driven, including satellite-based, estimates of ecosystem functioning and sensitivity to climate.

## 5. Summary and conclusions

Improved characterization of trait-based water use strategies is necessary as models shift from using coarse plant functional types toward incorporating plant traits, to better represent vegetation-climate feedbacks and ecological mechanisms in a changing climate (Matheny et al., 2017). Characterizing water use strategies remains uncertain, especially when aiming at effectively capturing ecosystem-scale water fluxes. This uncertainty is both conceptual, due to a lack of theoretical frameworks defining these strategies based on ecologically-meaningful outcomes, and operational, because eco-physiological models are complex and difficult to parameterize (Mencuccini et al., 2019).

We reduce the dimensionality of the problem by modeling long-term average dynamics of water fluxes through the SPAC using non-dimensional groups. We therefore define water use strategies without specifying individual traits, while still accounting for key eco-physiological mechanisms. These  $\Pi$  groups combine traits with environmental variables, thereby identifying fundamental axes of variation along which diverse trait-environment combinations can lead to similar outcomes in terms of water uptake capacity and water use performance. As such, our approach generalizes current metrics for water use strategies based solely on traits and improve our ability to effectively capture ecosystem-scale water fluxes. Furthermore, a primary  $\Pi$  group characterizing synchronization of plant water transport and atmospheric water demand, defines water use strategies.

Parameter estimates capturing observed soil moisture variability are consistent with those maximizing transpiration weighted by risks of water stress. This result supports ecohydrological optimality as a parsimonious guiding principle to assess water use strategies. We can thus infer water use strategies that are consistent with those encoded in soil moisture observations, and with more mechanistic underpinnings compared to exploratory data analysis. Using  $\Pi$  groups to link vegetation, soil and climatic conditions to optimal plant water use performance, we propose and validate a minimalist but transferable approach describing ecohydrological processes across climates and independently of scale.

#### Author contributions

MB, SM, and GV designed the research; MB performed the analysis and wrote the paper; SM and GV contributed to interpreting results, editing, and revising the paper.

#### Data availability statement

Code to reproduce the analysis in this study is available at <https://doi.org/10.5281/zenodo.5518546> and all necessary datasets are available at <https://fluxnet.org/data/fluxnet2015-dataset> and <https://fluxnet.org/data/fluxnet2015-dataset>

[://lpdaac.usgs.gov/products/mcd15a3hv006/](https://lpdaac.usgs.gov/products/mcd15a3hv006/).

## Declaration of Competing Interest

The authors declare that they have no known competing financial interests or personal relationships that could have appeared to influence the work reported in this paper.

## Acknowledgements

We thank Xue Feng, Trevor Keenan, Benjamin Blonder and several anonymous reviewers for feedback on earlier versions of the manuscript. MB thanks Stephen Good and Chad Higgins for discussions that inspired the study. MB and GV received funding from the European Commission and Swedish Research Council for Sustainable Development (FORMAS) (grant 2018-02787) in the frame of the international consortium iAquaduct financed under the 2018 Joint call of the WaterWorks2017 ERA-NET Cofund. GV was also supported by FORMAS (grant 2018-01820). MB used computational resources provided by the Swedish National Infrastructure for Computing at UPPMAX partially funded by the Swedish Research Council (grant 2018-05973). This work used data acquired and shared by the FLUXNET community.

## Supplementary materials

Supplementary material associated with this article can be found, in the online version, at [doi:10.1016/j.advwatres.2023.104405](https://doi.org/10.1016/j.advwatres.2023.104405).

## References

- Anderegg, W.R.L., 2015. Spatial and temporal variation in plant hydraulic traits and their relevance for climate change impacts on vegetation. *New Phytol.* 205, 1008–1014. <https://doi.org/10.1111/nph.12907>.
- Bassiouni, M., Good, S.P., Still, C.J., Higgins, C.W., 2020. Plant water uptake thresholds inferred from satellite soil moisture. *Geophys. Res. Lett.* 47, e2020GL087077 <https://doi.org/10.1029/2020GL087077>.
- Bassiouni, M., Higgins, C.W., Still, C.J., Good, S.P., 2018. Probabilistic inference of ecohydrological parameters using observations from point to satellite scales. *Hydrol. Earth Syst. Sci.* 22, 3229–3243. <https://doi.org/10.5194/hess-22-3229-2018>.
- Bassiouni, M., Vico, G., 2021. Parsimony vs predictive and functional performance of three stomatal optimization principles in a big-leaf framework. *New Phytol.* 231, 586–600. <https://doi.org/10.1111/nph.17392>.
- Bastiaanssen, W.G.M., Cheema, M.J.M., Immerzeel, W.W., Miltenburg, I.J., Pelgrum, H., 2012. Surface energy balance and actual evapotranspiration of the transboundary Indus Basin estimated from satellite measurements and the ETLook model. *Water Resour. Res.* 48, W11512. <https://doi.org/10.1029/2011WR010482>.
- Brooks, R.H., Corey, A.T., 1964. *Hydraulic Properties of Porous Media*. Colorado State University.
- Buckingham, E., 1914. On physically similar systems; illustrations of the use of dimensional equations. *Phys. Rev.* 4, 345–376. <https://doi.org/10.1103/PhysRev.4.345>.
- Budyko, M.I., 1974. *Climate and Life*. Academic Press.
- Caylor, K.K., D'Odorico, P., Rodriguez-Iturbe, I., 2006. On the ecohydrology of structurally heterogeneous semiarid landscapes. *Water Resour. Res.* 42, W07424. <https://doi.org/10.1029/2005WR004683>.
- Choat, B., Jansen, S., Brodribb, T.J., Cochard, H., Delzon, S., Bhaskar, R., Bucci, S.J., Feild, T.S., Gleason, S.M., Hacke, U.G., Jacobsen, A.L., Lens, F., Maherali, H., Martínez-Vilalta, J., Mayr, S., Mencuccini, M., Mitchell, P.J., Nardini, A., Pittermann, J., Pratt, R.B., Sperry, J.S., Westoby, M., Wright, I.J., Zanne, A.E., 2012. Global convergence in the vulnerability of forests to drought. *Nature* 491, 752–755. <https://doi.org/10.1038/nature11688>.
- Díaz, S., Kattge, J., Cornelissen, J.H.C., Wright, I.J., Lavorel, S., Dray, S., Reu, B., Kleyer, M., Wirth, C., Colin Prentice, I., Garnier, E., Bönsch, G., Westoby, M., Poorter, H., Reich, P.B., Moles, A.T., Dickie, J., Gillison, A.N., Zanne, A.E., Chave, J., Joseph Wright, S., Sheremet'ev, S.N., Jactel, H., Baraloto, C., Cerabolini, B., Pierce, S., Shipley, B., Kirkup, D., Casanoves, F., Joswig, J.S., Günther, A., Falczuk, V., Rüger, N., Mahecha, M.D., Gorné, L.D., 2016. The global spectrum of plant form and function. *Nature* 529, 167–171. <https://doi.org/10.1038/nature16489>.
- Dong, J., Akbar, R., Short Gianotti, D.J., Feldman, A.F., Crow, W.T., Entekhabi, D., 2022. Can surface soil moisture information identify evapotranspiration regime transitions? *Geophys. Res. Lett.* 49, e2021GL097697 <https://doi.org/10.1029/2021GL097697>.
- Dralle, D.N., Hahm, W.J., Rempe, D.M., Karst, N., Anderegg, L.D.L., Thompson, S.E., Dawson, T.E., Dietrich, W.E., 2020. Plants as sensors: vegetation response to rainfall predicts root-zone water storage capacity in Mediterranean-type climates. *Environ. Res. Lett.* 15, 104074 <https://doi.org/10.1088/1748-9326/abb10b>.
- Enquist, B.J., Norberg, J., Bonser, S.P., Violle, C., Webb, C.T., Henderson, A., Sloat, L.L., Savage, V.M., 2015. Chapter nine - scaling from traits to ecosystems: developing a general trait driver theory via integrating trait-based and metabolic scaling theories. In: Pawar, S., Woodward, G., Dell, A.I. (Eds.), *Advances in Ecological Research, Trait-Based Ecology - From Structure to Function*. Academic Press, pp. 249–318. <https://doi.org/10.1016/bs.aecr.2015.02.001>.
- Feddes, R.A., Kowalik, P.J., Zaradny, H., 1978. *Simulation of Field Water Use and Crop Yield, Simulation*. Centre for Agricultural Publishing and Documentation, Wageningen.
- Feng, X., Ackerly, D.D., Dawson, T.E., Manzoni, S., McLaughlin, B., Skelton, R.P., Vico, G., Weitz, A.P., Thompson, S.E., 2019. Beyond isohydrity: the role of environmental variability in determining plant drought responses. *Plant Cell Environ.* 42, 1104–1111. <https://doi.org/10.1111/pce.13486>.
- Feng, X., Ackerly, D.D., Dawson, T.E., Manzoni, S., Skelton, R.P., Vico, G., Thompson, S.E., 2018. The ecohydrological context of drought and classification of plant responses. *Ecol. Lett.* 21, 1723–1736. <https://doi.org/10.1111/ele.13139>.
- Feng, X., Dawson, T.E., Ackerly, D.D., Santiago, L.S., Thompson, S.E., 2017. Reconciling seasonal hydraulic risk and plant water use through probabilistic soil–plant dynamics. *Glob. Change Biol.* 23, 3758–3769. <https://doi.org/10.1111/gcb.13640>.
- Feng, X., Lu, Y., Jiang, M., Katul, G., Manzoni, S., Mrad, A., Vico, G., 2022. Instantaneous stomatal optimization results in suboptimal carbon gain due to legacy effects. *Plant Cell Environ.* 45, 3189–3204. <https://doi.org/10.1111/pce.14427>.
- Feng, X., Vico, G., Porporato, A., 2012. On the effects of seasonality on soil water balance and plant growth. *Water Resour. Res.* 48, W05543. <https://doi.org/10.1029/2011WR01263>.
- Franklin, O., Harrison, S.P., Dewar, R., Farrior, C.E., Brännström, Å., Dieckmann, U., Pietsch, S., Falster, D., Cramer, W., Loreau, M., Wang, H., Mäkelä, A., Rebel, K.T., Meron, E., Schymanski, S.J., Rovensky, E., Stocker, B.D., Zaehle, S., Manzoni, S., van Oijen, M., Wright, I.J., Ciais, P., van Bodegom, P.M., Peñuelas, J., Hofhansl, F., Terrer, C., Soudzilovskaia, N.A., Midgley, G., Prentice, I.C., 2020. Organizing principles for vegetation dynamics. *Nat. Plants* 6, 444–453. <https://doi.org/10.1038/s41477-020-0655-x>.
- Fu, X., Meinzer, F.C., 2019. Metrics and proxies for stringency of regulation of plant water status (iso/anisohydry): a global data set reveals coordination and trade-offs among water transport traits. *Tree Physiol.* 39, 122–134. <https://doi.org/10.1093/treephys/tpy087>.
- Fu, Z., Ciais, P., Feldman, A.F., Gentine, P., Makowski, D., Prentice, I.C., Stoy, P.C., Bastos, A., Wigneron, J.-P., 2022. Critical soil moisture thresholds of plant water stress in terrestrial ecosystems. *Sci. Adv.* 8, eabq7827. <https://doi.org/10.1126/sciadv.abq7827>.
- Good, S.P., Moore, G.W., Miralles, D.G., 2017. A mesic maximum in biological water use demarcates biome sensitivity to aridity shifts. *Nat. Ecol. Evol.* 1, 1883–1888. <https://doi.org/10.1038/s41559-017-0371-8>.
- Guswa, A.J., 2010. Effect of plant uptake strategy on the water–optimal root depth. *Water Resour. Res.* 46, W09601. <https://doi.org/10.1029/2010WR009122>.
- Guswa, A.J., 2008. The influence of climate on root depth: a carbon cost-benefit analysis. *Water Resour. Res.* 44, W02427. <https://doi.org/10.1029/2007WR006384>.
- Harrison, S.P., Cramer, W., Franklin, O., Prentice, I.C., Wang, H., Brännström, Å., de Boer, H., Dieckmann, U., Joshi, J., Keenan, T.F., Lavergne, A., Manzoni, S., Mengoli, G., Morfopoulos, C., Peñuelas, J., Pietsch, S., Rebel, K.T., Ryu, Y., Smith, N.G., Stocker, B.D., Wright, I.J., 2021. Eco-evolutionary optimality as a means to improve vegetation and land-surface models. *New Phytol.* 231, 2125–2141. <https://doi.org/10.1111/nph.17558>.
- Kannenbergh, S.A., Guo, J.S., Novick, K.A., Anderegg, W.R.L., Feng, X., Kennedy, D., Konings, A.G., Martínez-Vilalta, J., Matheny, A.M., 2022. Opportunities, challenges and pitfalls in characterizing plant water-use strategies. *Funct. Ecol.* 36, 24–37. <https://doi.org/10.1111/1365-2435.13945>.
- Kattge, J., Bönsch, G., Díaz, S., Lavorel, S., Prentice, I.C., Leadley, P., Tautenhahn, S., Werner, G.D.A., et al., 2020. TRY plant trait database – enhanced coverage and open access. *Glob. Change Biol.* 26, 119–188. <https://doi.org/10.1111/gcb.14904>.
- Konings, A.G., Gentine, P., 2017. Global variations in ecosystem-scale isohydrity. *Glob. Change Biol.* 23, 891–905. <https://doi.org/10.1111/gcb.13389>.
- Laio, F., Porporato, A., Ridol, L., Rodriguez-Iturbe, I., 2001. Plants in water-controlled ecosystems: active role in hydrologic processes and response to water stress II. Probabilistic soil moisture dynamics. *Adv. Water Resour.* 24, 707–723. [https://doi.org/10.1016/S0309-1708\(01\)00005-7](https://doi.org/10.1016/S0309-1708(01)00005-7).
- Lavergne, A., Graven, H., Kauwe, M.G.D., Keenan, T.F., Medlyn, B.E., Prentice, I.C., 2019. Observed and modelled historical trends in the water-use efficiency of plants and ecosystems. *Glob. Change Biol.* 25, 2242–2257. <https://doi.org/10.1111/gcb.14634>.
- Liu, Y., Holtzman, N.M., Konings, A.G., 2021a. Global ecosystem-scale plant hydraulic traits retrieved using model-data fusion. *Hydrol. Earth Syst. Sci.* 25, 2399–2417. <https://doi.org/10.5194/hess-25-2399-2021>.
- Liu, Y., Konings, A.G., Kennedy, D., Gentine, P., 2021b. Global coordination in plant physiological and rooting strategies in response to water stress. *Global Biogeochem. Cycles* 35, e2020GB006758. <https://doi.org/10.1029/2020GB006758>.
- Liu, Y., Kumar, M., Katul, G.G., Feng, X., Konings, A.G., 2020. Plant hydraulics accentuates the effect of atmospheric moisture stress on transpiration. *Nat. Clim. Chang.* 10, 691–695. <https://doi.org/10.1038/s41558-020-0781-5>.
- Lu, Y., Duursma, R.A., Farrior, C.E., Medlyn, B.E., Feng, X., 2020. Optimal stomatal drought response shaped by competition for water and hydraulic risk can explain plant trait covariation. *New Phytol.* 225, 1206–1217. <https://doi.org/10.1111/nph.16207>.
- Lu, Y., Duursma, R.A., Medlyn, B.E., 2016. Optimal stomatal behaviour under stochastic rainfall. *J. Theor. Biol.* 394, 160–171. <https://doi.org/10.1016/j.jtbi.2016.01.003>.

- Manzoni, S., Vico, G., Katul, G., Palmroth, S., Jackson, R.B., Porporato, A., 2013a. Hydraulic limits on maximum plant transpiration and the emergence of the safety-efficiency trade-off. *New Phytol.* 198, 169–178. <https://doi.org/10.1111/nph.12126>.
- Manzoni, S., Vico, G., Katul, G., Palmroth, S., Porporato, A., 2014. Optimal plant water-use strategies under stochastic rainfall. *Water Resour. Res.* 50, 5379–5394. <https://doi.org/10.1002/2014WR015375>.
- Manzoni, S., Vico, G., Porporato, A., Katul, G., 2013b. Biological constraints on water transport in the soil–plant–atmosphere system. *Adv. Water Resour.* 51, 292–304. <https://doi.org/10.1016/j.advwatres.2012.03.016>.
- Matheny, A.M., Mirfenderesgi, G., Bohrer, G., 2017. Trait-based representation of hydrological functional properties of plants in weather and ecosystem models. *Plant Divers.* 39, 1–12. <https://doi.org/10.1016/j.pld.2016.10.001>.
- Meinzer, F.C., Woodruff, D.R., Marias, D.E., Smith, D.D., McCulloh, K.A., Howard, A.R., Magedman, A.L., 2016. Mapping ‘hydroscares’ along the iso- to anisohydric continuum of stomatal regulation of plant water status. *Ecol. Lett.* 19, 1343–1352. <https://doi.org/10.1111/ele.12670>.
- Mencuccini, M., Manzoni, S., Christoffersen, B., 2019. Modelling water fluxes in plants: from tissues to biosphere. *New Phytol.* 222, 1207–1222. <https://doi.org/10.1111/nph.15681>.
- Mencuccini, M., Minunno, F., Salmon, Y., Martínez-Vilalta, J., Hölttä, T., 2015. Coordination of physiological traits involved in drought-induced mortality of woody plants. *New Phytol.* 208, 396–409. <https://doi.org/10.1111/nph.13461>.
- Migliavacca, M., Musavi, T., Mahecha, M.D., Nelson, J.A., Knauer, J., Baldocchi, D.D., Perez-Priego, O., Christiansen, R., Peters, J., Anderson, K., Bahn, M., Black, T.A., Blanken, P.D., Bonal, D., Buchmann, N., Caldararu, S., Carrara, A., Carvalhais, N., Cescatti, A., Chen, J., Cleverly, J., Cremonese, E., Desai, A.R., El-Madany, T.S., Farella, M.M., Fernández-Martínez, M., Filippa, G., Forkel, M., Galvagno, M., Gomasasca, U., Gough, C.M., Göckede, M., Ibrom, A., Ikawa, H., Janssens, I.A., Jung, M., Kattge, J., Keenan, T.F., Knohl, A., Kobayashi, H., Kraemer, G., Law, B.E., Liddell, M.J., Ma, X., Mammarella, I., Martini, D., Macfarlane, C., Matteucci, G., Montagnani, L., Pabon-Moreno, D.E., Panigada, C., Papale, D., Pendall, E., Penuelas, J., Phillips, R.P., Reich, P.B., Rossini, M., Rotenberg, E., Scott, R.L., Stahl, C., Weber, U., Wohlfahrt, G., Wolf, S., Wright, I.J., Yakir, D., Zaehle, S., Reichstein, M., 2021. The three major axes of terrestrial ecosystem function. *Nature* 598, 468–472. <https://doi.org/10.1038/s41586-021-03939-9>.
- Myneni, R., Knyazikhin, Y., Park, T., 2015. MCD15A3H MODIS/Terra+Aqua Leaf Area Index/FPAR 4-day L4 Global 500 m SIN Grid V006. <https://doi.org/10.5067/MODIS/MCD15A3H.006>.
- Paschalis, A., Faticchi, S., Pappas, C., Or, D., 2018. Covariation of vegetation and climate constrains present and future T/ET variability. *Environ. Res. Lett.* 13, 104012. <https://doi.org/10.1088/1748-9326/aae267>.
- Pastorello, G., Trotta, C., Canfora, E., Chu, H., Christianson, D., Cheah, Y.-W., Poindexter, C., Chen, J., Elbashedy, A., Humphrey, M., Isaac, P., Polidori, D., Ribeca, A., van Ingen, C., Zhang, L., et al., 2020. The FLUXNET2015 dataset and the ONEFlux processing pipeline for eddy covariance data. *Sci. Data* 7, 225. <https://doi.org/10.1038/s41597-020-0534-3>.
- Porporato, A., 2022. Hydrology without dimensions. *Hydrol. Earth Syst. Sci.* 26, 355–374. <https://doi.org/10.5194/hess-26-355-2022>.
- Porporato, A., Daly, E., Rodríguez-Iturbe, I., 2004. Soil water balance and ecosystem response to climate change. *Am. Nat.* 164, 625–632. <https://doi.org/10.1086/424970>.
- Porporato, A., Laio, F., Ridol, L., Rodríguez-Iturbe, I., 2001. Plants in water-controlled ecosystems: active role in hydrologic processes and response to water stress III. Vegetation water stress. *Adv. Water Resour.* 20, 725–744. [https://doi.org/10.1016/S0309-1708\(01\)00006-9](https://doi.org/10.1016/S0309-1708(01)00006-9).
- Prentice, I.C., Dong, N., Gleason, S.M., Maire, V., Wright, I.J., 2014. Balancing the costs of carbon gain and water transport: testing a new theoretical framework for plant functional ecology. *Ecol. Lett.* 17, 82–91. <https://doi.org/10.1111/ele.12211>.
- Prentice, I.C., Liang, X., Medlyn, B.E., Wang, Y.-P., 2015. Reliable, robust and realistic: the three R’s of next-generation land-surface modelling. *Atmosph. Chem. Phys.* 15, 5987–6005. <https://doi.org/10.5194/acp-15-5987-2015>.
- Priestley, C.H.B., Taylor, R.J., 1972. On the assessment of surface heat flux and evaporation using large-scale parameters. *Monthly Weather Rev.* 100, 81–92. [https://doi.org/10.1175/1520-0493\(1972\)100<0081:OTAOSH>2.3.CO;2](https://doi.org/10.1175/1520-0493(1972)100<0081:OTAOSH>2.3.CO;2).
- Reich, P.B., 2014. The world-wide ‘fast–slow’ plant economics spectrum: a traits manifesto. *J. Ecol.* 102, 275–301. <https://doi.org/10.1111/1365-2745.12211>.
- Rodríguez-Iturbe, I., Porporato, A., 2005. *Ecology of Water-Controlled Ecosystems: Soil Moisture and Plant Dynamics*. Cambridge University Press, Cambridge.
- Sabot, M.E.B., De Kauwe, M.G., Pitman, A.J., Medlyn, B.E., Ellsworth, D.S., Martin-StPaul, N.K., Wu, J., Choat, B., Limousin, J.-M., Mitchell, P.J., Rogers, A., Serbin, S. P., 2022. One stomatal model to rule them all? Toward improved representation of carbon and water exchange in global models. *J. Adv. Model. Earth Syst.* 14, e2021MS002761. <https://doi.org/10.1029/2021MS002761>.
- Scheiter, S., Langan, L., Higgins, S.I., 2013. Next-generation dynamic global vegetation models: learning from community ecology. *New Phytol.* 198, 957–969. <https://doi.org/10.1111/nph.12210>.
- Skelton, R.P., West, A.G., Dawson, T.E., 2015. Predicting plant vulnerability to drought in biodiverse regions using functional traits. *Proc. Natl. Acad. Sci. USA* 112, 5744–5749. <https://doi.org/10.1073/pnas.1503376112>.
- Sloan, B.P., Thompson, S.E., Feng, X., 2021. Plant hydraulic transport controls transpiration sensitivity to soil water stress. *Hydrol. Earth Syst. Sci.* 25, 4259–4274. <https://doi.org/10.5194/hess-25-4259-2021>.
- Stocker, B.D., Tumber-Dávila, S.J., Konings, A.G., Anderson, M.B., Hain, C., Jackson, R. B., 2023. Global patterns of water storage in the rooting zones of vegetation. *Nat. Geosci.* <https://doi.org/10.1038/s41561-023-01125-2>.
- Trugman, A.T., Anderegg, L.D.L., Shaw, J.D., Anderegg, W.R.L., 2020. Trait velocities reveal that mortality has driven widespread coordinated shifts in forest hydraulic trait composition. *PNAS* 117, 8532–8538. <https://doi.org/10.1073/pnas.1917521117>.
- Wang, L., Good, S.P., Caylor, K.K., 2014. Global synthesis of vegetation control on evapotranspiration partitioning. *Geophys. Res. Lett.* 41, 6753–6757. <https://doi.org/10.1002/2014GL061439>.
- Wang, Y., Sperry, J.S., Anderegg, W.R.L., Venturas, M.D., Trugman, A.T., 2020. A theoretical and empirical assessment of stomatal optimization modeling. *New Phytol.* 227, 311–325. <https://doi.org/10.1111/nph.16572>.
- Wei, Z., Yoshimura, K., Wang, L., Miralles, D.G., Jasechko, S., Lee, X., 2017. Revisiting the contribution of transpiration to global terrestrial evapotranspiration: revisiting Global ET Partitioning. *Geophys. Res. Lett.* 44, 2792–2801. <https://doi.org/10.1002/2016GL072235>.